**SANDIA REPORT**
SAND2010-8704
Unlimited Release
Printed December 2010

# Thermal Stability and Adhesion of Low-Emissivity Electroplated Au Coatings

Nancy Yang, Jeff Jorenby, W. Miles Clift, John Hachman, and Jeff Chames

Prepared by
Sandia National Laboratories
Albuquerque, New Mexico 87185 and Livermore, California 94550

Sandia National Laboratories is a multi-program laboratory managed and operated by Sandia Corporation, a wholly owned subsidiary of Lockheed Martin Corporation, for the U.S. Department of Energy's National Nuclear Security Administration under contract DE-AC04-94AL85000.



Issued by Sandia National Laboratories, operated for the United States Department of Energy by Sandia Corporation.



Available to DOE and DOE contractors from
U.S. Department of Energy
Office of Scientific and Technical Information
P.O. Box 62
Oak Ridge, TN 37831

Telephone: (865) 576-8401
Facsimile: (865) 576-5728
E-Mail: reports@adonis.osti.gov
Online ordering: http://www.osti.gov/bridge

Available to the public from
U.S. Department of Commerce
National Technical Information Service
5285 Port Royal Rd.
Springfield, VA 22161

Telephone: (800) 553-6847
Facsimile: (703) 605-6900
E-Mail: orders@ntis.fedworld.gov
Online order: http://www.ntis.gov/help/ordermethods.asp?loc=7-4-0#online

SAND2010-8704
Unlimited Release
Printed December 2010

# Thermal Stability and Adhesion of Low-Emissivity Electroplated Au Coatings

Nancy Yang, Jeff Jorenby, W. Miles Clift, John Hachman, and Jeff Chames
Energy Nanomaterials, 8651
Sandia National Laboratories
P.O. Box 969
Livermore, CA. 94551-0969

## Abstract

We are developing a low-emissivity thermal management coating system to minimize radiative heat losses under a high-vacuum environment. Good adhesion, low outgassing, and good thermal stability of the coating material are essential elements for a long-life, reliable thermal management device. The system of electroplated Au coating on the adhesion-enhancing Wood's Ni strike and 304L substrate was selected due to its low emissivity and low surface chemical reactivity.

The physical and chemical properties, interface bonding, thermal aging, and compatibility of the above Au/Ni/304L system were examined extensively. The study shows that the as-plated electroplated Au and Ni samples contain submicron columnar grains, stringers of nanopores, and/or $H_2$ gas bubbles, as expected. The grain structure of Au and Ni are thermally stable up to 250°C for 63 days. The interface bonding is strong, which can be attributed to good mechanical locking among the Au, the 304L, and the porous Ni strike. However, thermal instability of the nanopore structure (i.e., pore coalescence and coarsening due to vacancy and/or entrapped gaseous phase diffusion) and Ni diffusion were observed. In addition, the study also found that prebaking 304L in the furnace at $\geq 1 \times 10^{-4}$ Torr promotes surface Cr-oxides on the 304L surface, which reduces the effectiveness of the intended H-removal. The extent of the pore coalescence and coarsening and their effect on the long-term system integrity and outgassing are yet to be understood.

Mitigating system outgassing and improving Au adhesion require a further understanding of the process–structure–system performance relationships within the electroplated Au/Ni/304L system.

This page intentionally left blank.

# Contents

# Figures

# Tables

# Acknowledgments

The authors thank Bernice Mills, Alfred Morales, and Terry Johnson for their technical discussions and inputs for this report. Thanks also go to Davina Kwon, Tim Sheppod, Bill Even, and Sarah Allendorf for their management support of the project.

# 1 Introduction

Research and development effort are currently underway at SNL/CA to develop a low-emissivity metal coating for thermal management of powder source devices. Electroplated Au coating has been down-selected for its relatively low emissivity (Table 1) and relatively low surface oxidation. An electroplating process for a low-emissivity Au coating with cyanide electrolytic bath, developed by Org. 8223, was selected due to the good adhesion and thermally stable microstructure relative to those coatings plated in a sulfite bath (Figure 1 (a–b)). There are other material issues associated with gold-plated nickel used for electronic packaging applications were discussed by others, e.g., the presence of $H_2$ gas and Ni/Au interdiffusion at elevated temperature (Ref. 1–4). Many of the issues discussed in this paper may be relevant for our application; however, they are beyond the scope of this study.

To ensure a long-term reliable Au/Ni/304L system based on sound science, an extensive materials science examination and characterization was performed. The scientific study included physical and chemical characteristics, interface bonding, and thermal stability and its evolution. Such scientific information shall allow us to determine the achievable specifications with a feasible electroplating process. In this report, we present and discuss the details of the scientific findings and their implications to system performance.

**Table 1.** Emissivity (ε) of different metals.

| Metal | Exp. ε | Ideal ε |
|---|---|---|
| Stainless Steels | 0.12 (SNL) | 0.098 |
| Nickel | 0.04 | 0.033 |
| Aluminum | 0.02 | 0.019 |
| Silver | 0.015 | 0.016 |
| Copper | 0.027 | 0.015 |
| Gold | 0.02 (SNL) | 0.007 |

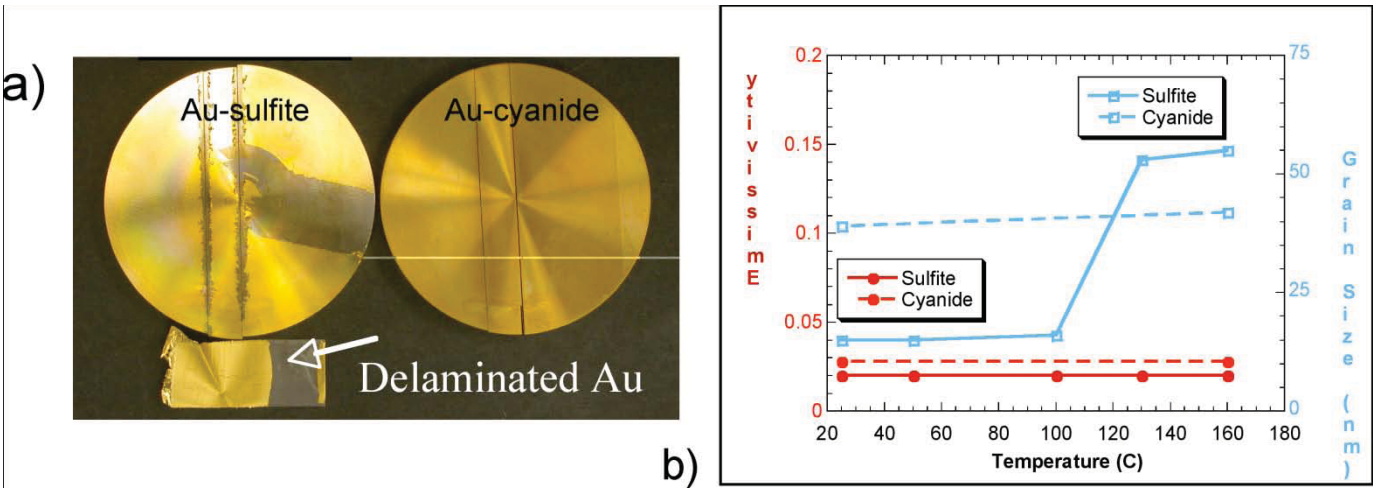


**Figure 1.** (a) Scotch tape test showing good adhesion of Au–cyanide (right) and delaminated Au–sulfite (left); (b) Grain-size data showing the more stable grain structure of Au plated in cyanide than in the sulfite bath, which has undergone grain growth at the annealing temperature (≥100°C).

# 2 Experiments

## 2.1 Materials

Six 304L stainless steel pucks used for the current Au and Ni electroplating study measured 2 in. in diameter and ¼ in. thick, as shown in the digital images in Figure 2. The fabrication process and thermal history for each sample are described in Table 2. Samples A2 and B2 are the as-received 304L blanks. Samples A2+Ni strike and B2+Ni strike contain only Wood's Ni strike (nominal 300 nm thick), plated on a small piece cut from the A2 and B2 blanks. Samples A1 and B1 contain Au (nominal 1.0 µm thick) plated on the Ni strike in the cyanide bath at SNL/CA. Three A-type samples were as received without the initial 304L prebake. Three B-type samples had received the 304L prebake at 400°C/5 days to remove hydrogen from the 304L pucks. The 304L prebake step is designed to mitigate possible system outgassing. Discoloration was noticed on the sample B2 blank upon prebake.

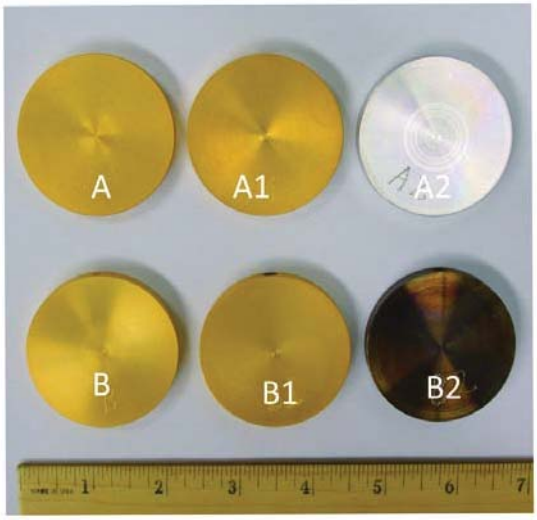


**Figure 2.** Digital photography shows the dimensions of the six as-received pucks.

**Table 2.** Sample fabrication processing and thermal history.

| | |
|---|---|
| **A2: 304L blank**<br>-As-received 304L puck | **B2: 304L blank**<br>-Prebaked 304L puck at 400°C/5 days |
| **A1: Au plated**<br>-As received 304L puck<br>-Electroplated Au w/Ni strike | **B1: Au plated**<br>-Pre-baked 304L puck at 400°C/5 days<br>-Electroplated Au w/ Ni strike |
| **A: Au plated**<br>- As-received 304L puck<br>- Electroplated Au w/ Ni strike<br>- Bake the entire component at:<br>100°C for 7 days at 10x-4 Torr | **B: Au plated**<br>-Prebaked 304L puck at 400°C/5 days<br>-Electroplated Au w/ Ni strike<br>-Bake the entire component at:<br>100°C/7days at 10x-4 torr |
| **A1+190°C: Au plated**<br>- As-received 304L puck<br>- Electroplated Au w/ Ni strike<br>- Bake the entire component at:<br>190°C for 7 days at 10x-4 torr | **B1+190°C: Au plated**<br>-Prebaked 304L puck at 400°C/5 days<br>-Electroplated Au w/ Ni strike<br>-Bake the entire component at:<br>190°C/7days at 10x-4 torr |
| **A1+250°C Au plated**<br>- As-received 304L puck<br>- Electroplated Au w/ Ni strike<br>- Bake the entire component at:<br>250°C for 63 days at 10x-4 torr | **B1+250°C Au plated**<br>- As-received 304L puck<br>- Electroplated Au w/ Ni strike<br>- Bake the entire component at:<br>250°C for 63 days at 10x-4 torr |
| **A2+Ni strike**<br>-As-received 304L puck<br>-Electroplated Ni-strike | **B2+Ni Strike**<br>-Prebaked 304L puck<br>-Electroplated Ni-strike |

## 2.2 Electroplating procedure

The electroplating procedures and conditions, including initial surface preparation and treatment prior to the Au and Ni electroplate, are described below in Table 3.

**Table 3.** Electroplating procedure and conditions.

1. Caustic clean 15 min
2. DI Water rinse
3. 30% by volume Nitric acid pickle dip 30 sec
4. DI Water rinse
5. Anodic etch in 30% sulfuric acid @ 150 ASF ( Amps per Square Foot) for 3 minutes
6. DI Water rinse
7. Woods Nickel strike @ 50 ASF for 5 minutes
8. DI Water rinse
9. Gold plate in the Au-cyanide bath @ 1.5 ma/cm2 for 10 minutes = 1 µm
10. DI Water rinse
11. Blow dry with Dry Nitrogen

Note: The $H_2SO_4$ etch in the step 5 shall remove all foreign contaminants, including residues from air born and/or mechanical handling as well as surface oxide generated from thermal annealing

This page intentionally left blank.

# 3 Material Characterization Techniques

- **Microstructure and surface morphology:** The analyses were conducted using a combination of advanced electron optical imaging techniques, including optical metallography, scanning electron microscopy (SEM), dual beam focused ion beam (FIB) with SEM, and transmission electron microscopy (TEM).
- **Chemical composition:** The analyses were conducted using a combination of SEM with energy dispersive *x*-ray spectroscopy (EDS), Auger electron spectroscopy (AEM), and TEM with EDS.

  The submicron surface chemical composition and the composition depth profile were analyzed using AEM by Physical Electronics Model 680 with typical e-beam parameters of 5.0 keV at 20 nA, rastered over a 100-µm x 100-µm area. Sputter Auger profiling was done using a 2-keV $Ar^+$ ion beam at a 45° angle of incidence, rastered over a 800-µm x 800-µm area. The experimental measurement technique is illustrated schematically in Figure 3 below.
- **Coating adhesion:** The adhesion strength of the Au coatings onto the 304L substrate with Ni strike was qualitatively estimated using a simple Scotch tape pull test.

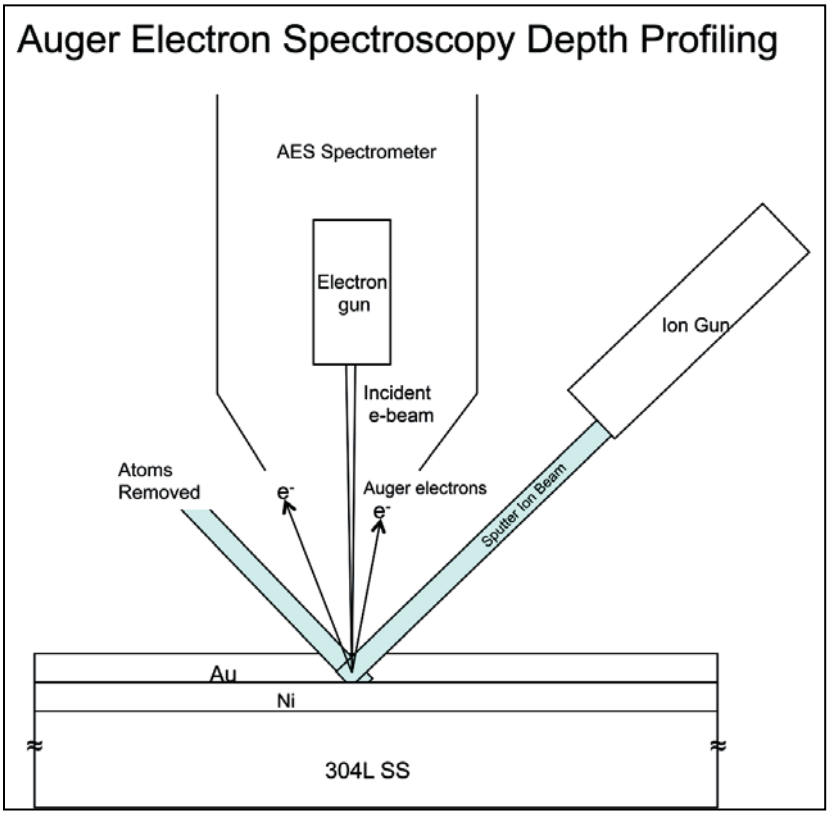


**Figure 3.** Schematic of the Auger electron depth profiling.

This page intentionally left blank.

# 4 Experimental Results

The extensive material characterization of ten Au/Ni/304L systems (five for A-type and five for B-type) yielded a large volume of experimental data and results. These extensive experimental results indicate little difference in the initial physical and chemical properties as well as the thermal evolution between the A- and B-types. The prebake step seems to have minimal effect on the physical and chemical properties being discussed in this report.

In order to make the report easier to follow, in many cases, the data illustration and discussion are focused on one of the two types (A- or B-type) rather than both.

## 4.1 Surface morphology

SEM images in Figure 4 show typical surface contour and morphology on each puck. These contours mimic mechanical surface finishing on the substrate beneath the submicrometer Au and Ni coatings. These images clearly show the variation in surface contour and morphology among the six pucks, which is indicative of variations in the mechanical machining finish. In addition to the variation in surface contours, the SEM images at higher magnification also show surface defects, i.e., satellite pits, primarily on the B1 puck (Figure 5–6, arrows).

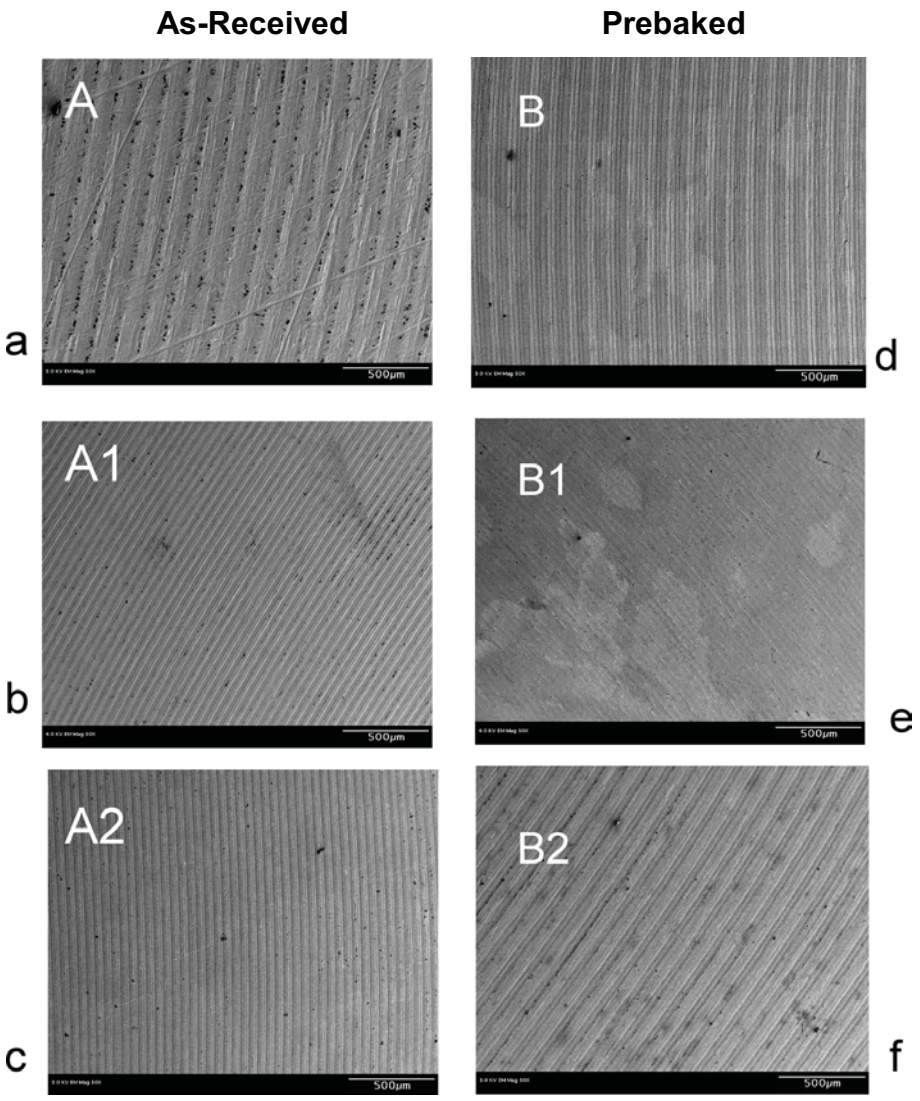


**Figure 4.** SEM images showing the variation in surface contour among the six pucks due to inconsistent mechanical machining finish.

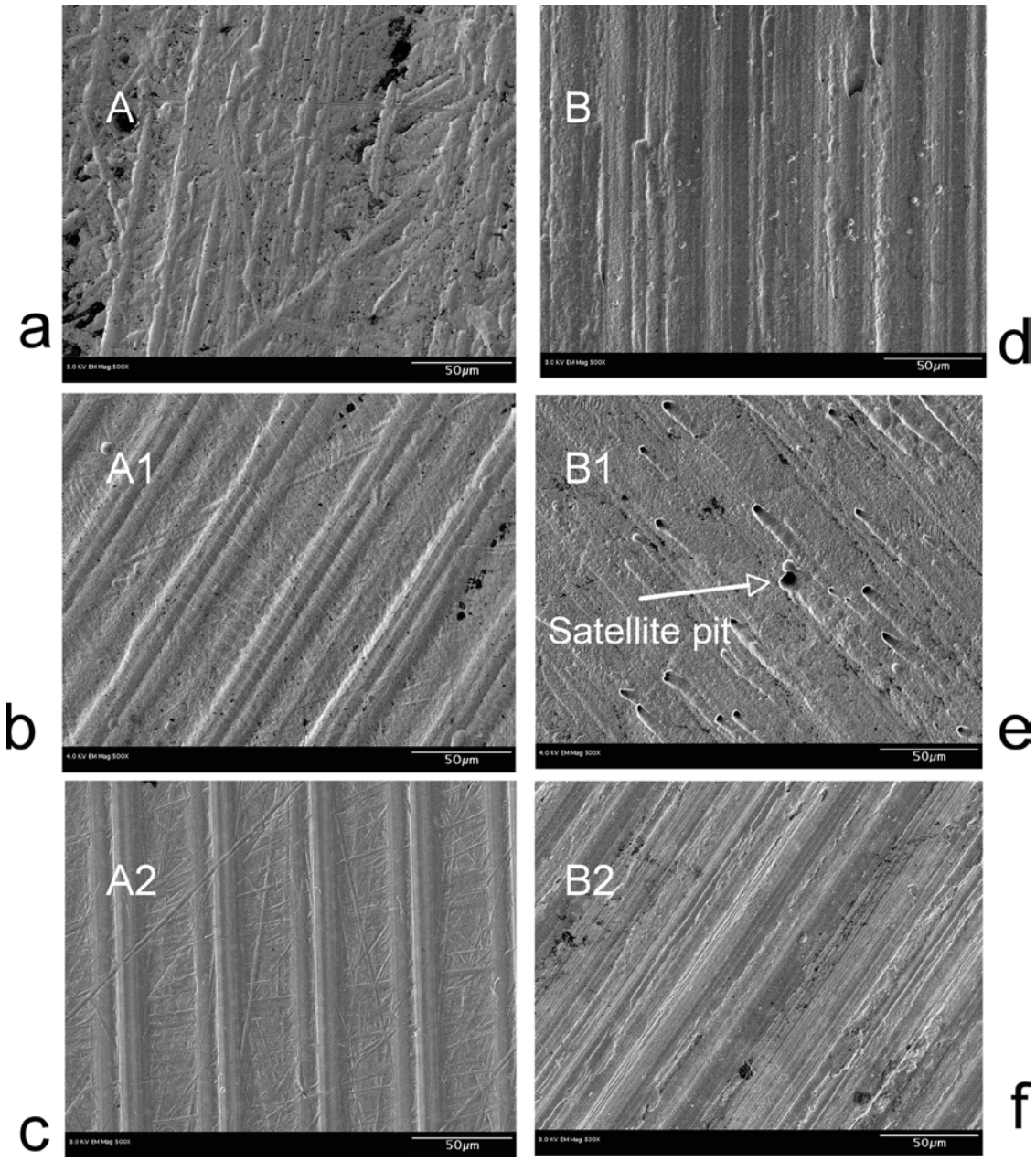


**Figure 5.** SEM images at higher magnification showing details of the roughened surface contour and the large pits along the machining marks (see arrow).

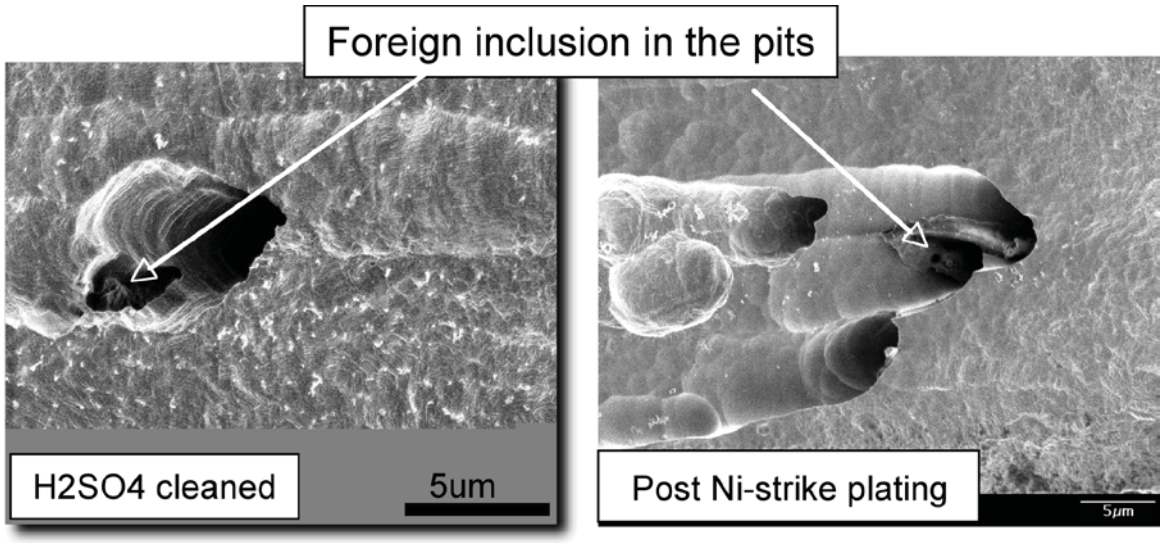


**Figure 6.** SEM images showing the foreign substance trapped deep inside the surface pits after sulfuric acid cleaning.

## 4.2 Surface chemical analyses of the blanks

### *4.2.1 Before sulfuric acid ($H_2SO_4$) cleaning*

The most noticeable difference between the as-machined (A2) and 400°C prebaked (B2) blanks is the discoloration observed on the 400°C prebaked puck (Figure 7, lower left). The SEM images show that the discolored B2 surface contains dense aggregates of surface deposits (Figure 7, lower middle arrows) that were not seen on the as-machined A2 (Figure 7, upper middle). EDS analyses identified the surface deposit as Cr-oxides, as shown in the EDS spectrum and the Cr and O *x*-ray maps in Figure 8. The presence of Fe in the EDS spectrum is an artifact of the characteristic 304L substrate beneath the Cr-oxide deposits. Auger depth profiling of the as-received and prebaked pucks show the formation of a thin surface Cr-oxide, with average thickness of ~25 nm, on the discolored prebaked B2 puck (Figure 9, arrows).

### *4.2.2 After $H_2SO_4$ cleaning*

Sulfuric acid ($H_2SO_4$) cleaning is a standard procedure that is intended to remove all surface contamination prior to electroplating. In the current Au/Ni electroplating, the SEM images in Figure 8 show that $H_2SO_4$ cleaning removed the majority of the Cr-oxides as, expected, with the exception of a few remnants (Figure 7, lower right arrow).

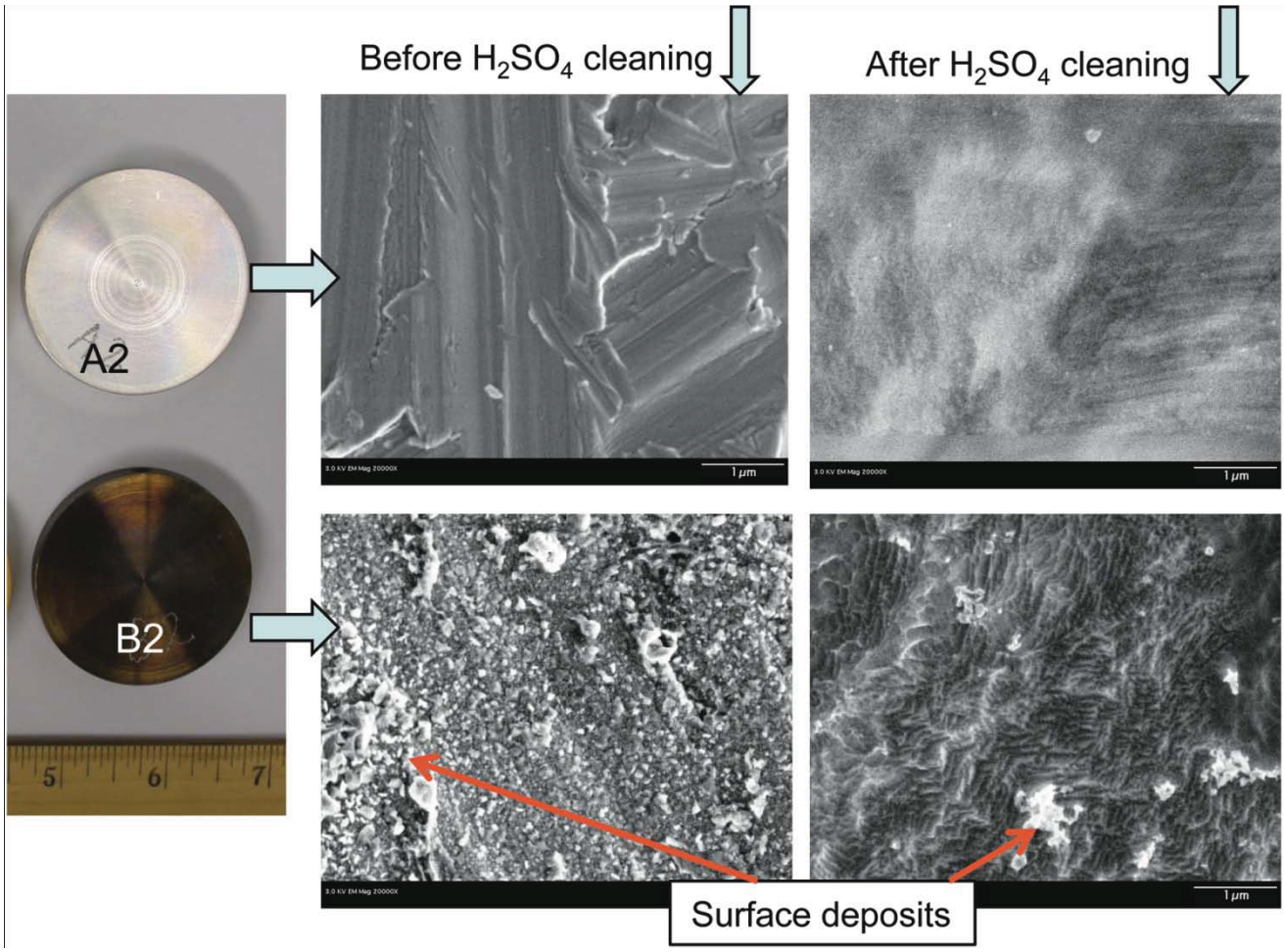


**Figure 7.** SEM images showing surface characteristics of the blanks before and after $H_2SO_4$ cleaning. Upper row: as-machined blank A2; lower row: 400°C prebaked blank B2.

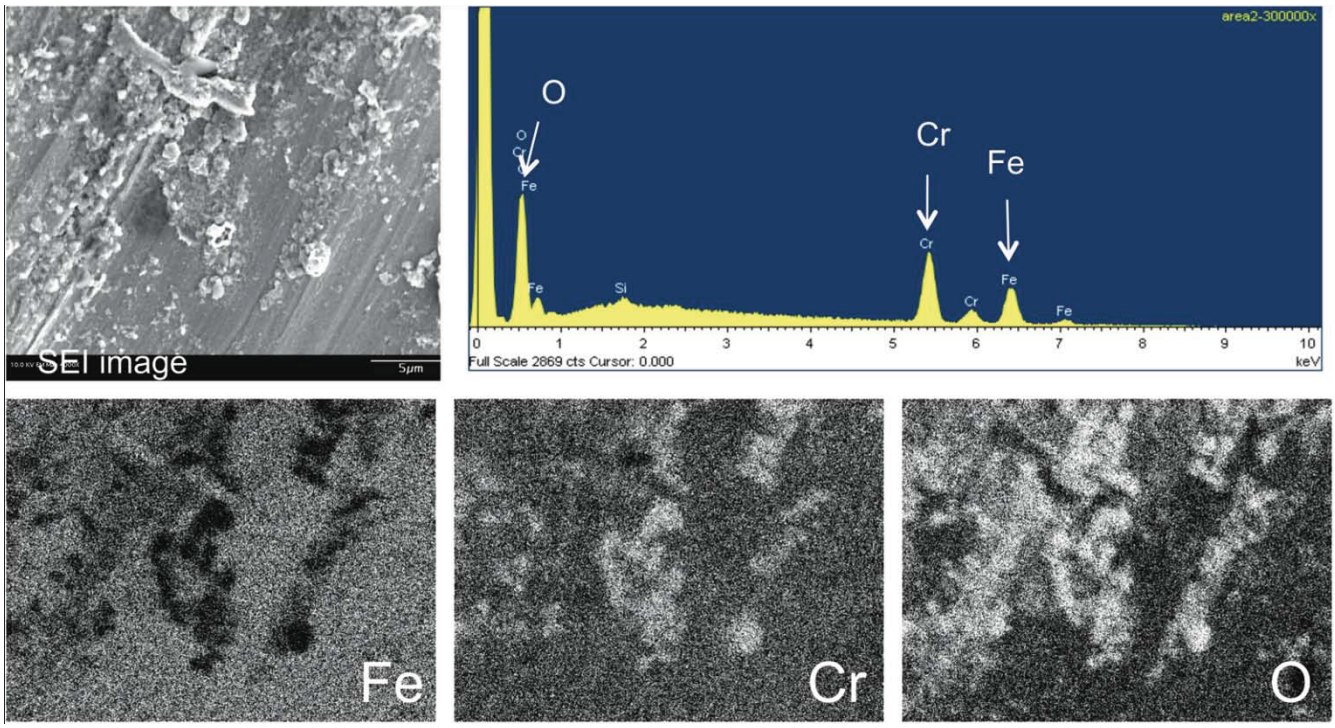


**Figure 8.** SEM/EDS spectrum and *x*-ray maps from the surface deposit on B2 400°C prebaked. Upper left is an SEM image of the surface deposit; Upper right is an EDS spectrum showing a strong presence of Cr and oxygen; Lower images are Fe, Cr and O *x*-ray maps showing enrichment of Cr and O in the surface deposits, which is indicative of formation of surface Cr-oxide.

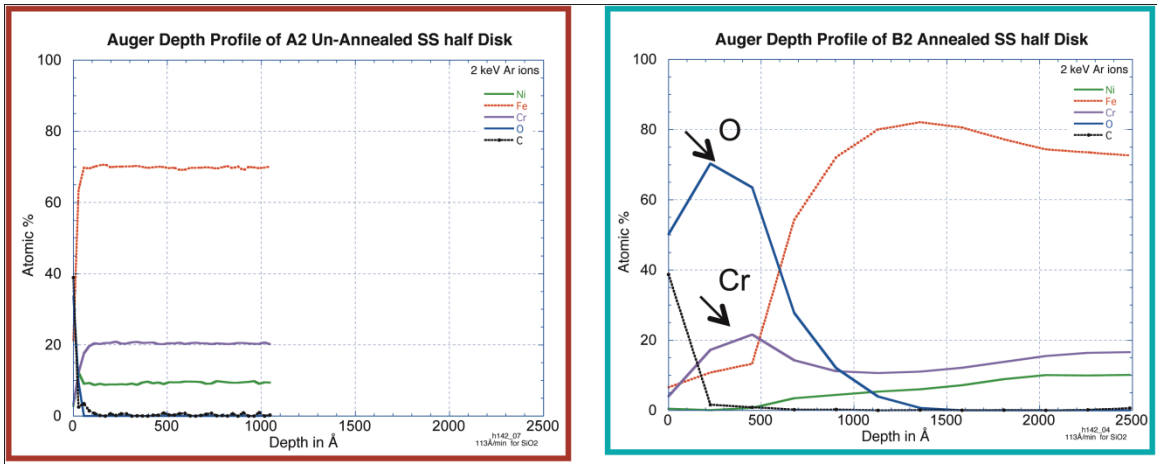


**Figure 9.** Auger electron profiles of the as-plated A-type sample (left) and 400°C/5 days prebaked B-type samples (right). Surface Cr-oxide, ~ 25 nm thick, was detected.

## 4.3 Surface morphology of the Wood's Ni strike

Since a Ni strike serves as an adhesion enhancer, its surface morphology (or roughness) as well as porosity become important factors for Au adhesion. The typical Wood's Ni strike surface morphology was examined by SEM imaging. The results show that the surface structure of the electroplated Ni strike contains extremely fine columnar grains, << 200 nm wide (Figure 10, right column). Variation in the Ni grain morphology and size between the A2 and B2 puck was observed. The as-machined $H_2SO_4$-cleaned 304L A2 surface is relatively smooth, leading to a thin, higher aspect-ratio, columnar Ni deposit (Figure 10, upper row). On the other hand, the surface of the prebaked $H_2SO_4$-cleaned B2 304L surface was faceted, leading to a more equiaxed Ni deposit (Figure 10, lower row). This difference suggests a variation in the combination of the initial mechanical machining finish and the subsequent Ni strike grain structure (Figure 10, left).

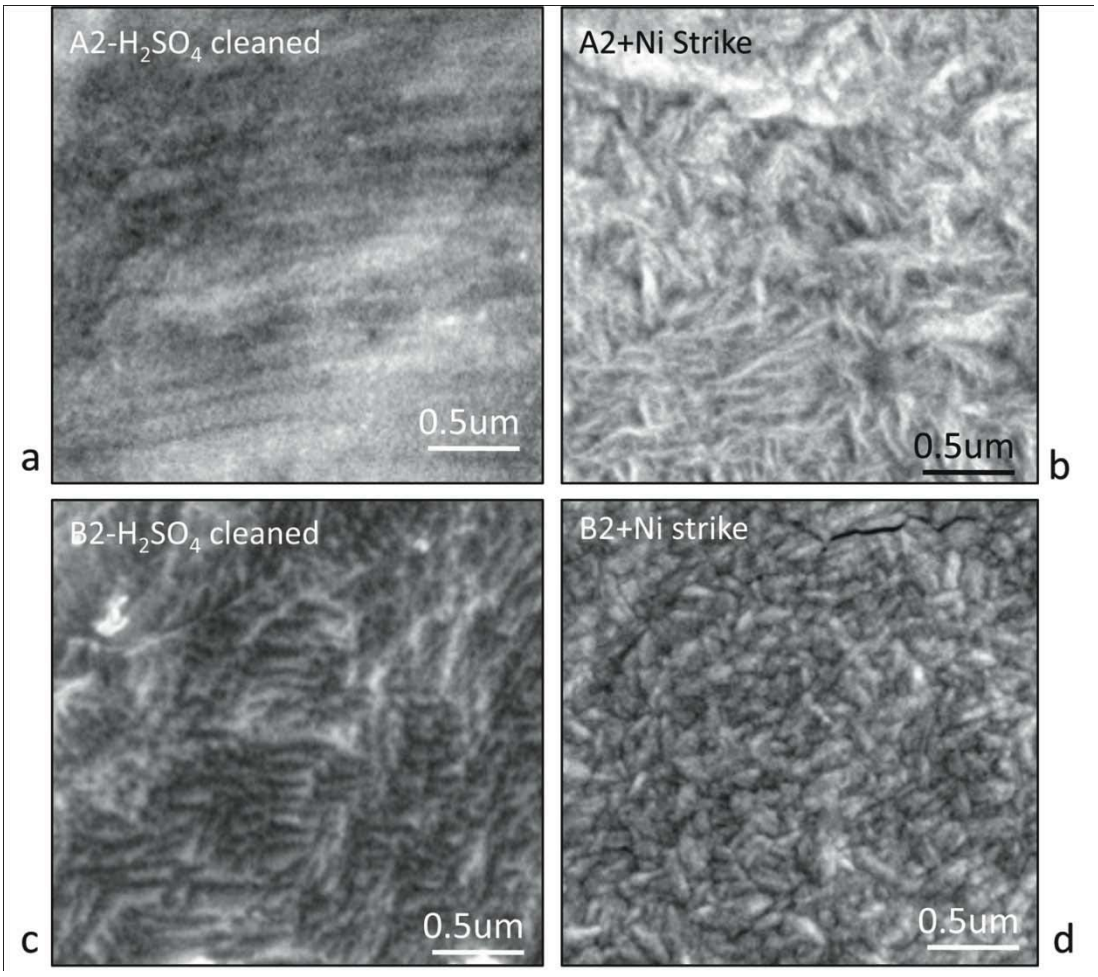


**Figure 10.** SEM images showing the difference in surface morphology of the 304L substrate before and after $H_2SO_4$ cleaning and the resulting surface morphology of the Ni strikes.

## 4.4 Optical metallographic and FIB imaging of Au coating cross-sections

An optical image of the metallographic-polished puck cross-section shows an extremely thin and wavy submicron Au coating on the rough surface of the 304L substrate (Figure 11a). The FIB image at higher magnification (see Figure 11a, circled area) shows the typical construction and dimension of the Au coating with Wood's Ni strike layer on the 304L substrate (Figure 11b). The thicknesses of the Au coating and the Ni strike layer, estimated from the FIB image, are ~400–500 nm and 200–300 nm, respectively. The grain structure of both the electroplated Au and Ni are also submicrometer in size.

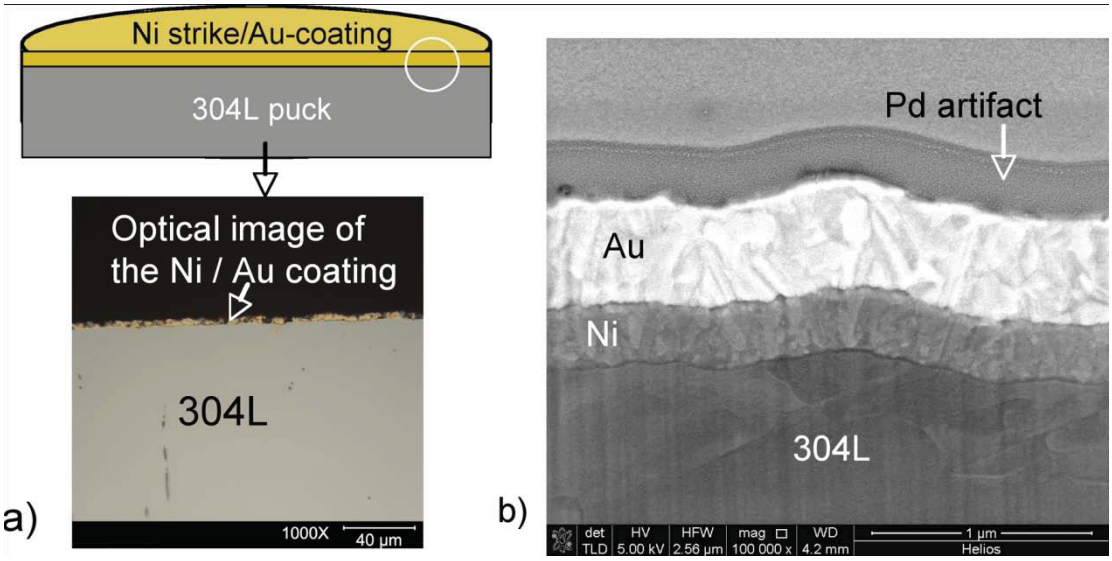


**Figure 11.** (a) Schematic (upper) and optical image (lower) of the metallographic polished Au/Ni coating cross-section; (b) FIB images of the thin-sliced FIB cross-section.

## 4.5 Au coating adhesion

A simple Scotch tape pull test was conducted to estimate Au coating adhesion strength qualitatively. The results show that all four Au coatings regardless of their prebaking history exhibit good adhesion. Compared with those Au coatings plated in the sulfite bath with poor adhesion described in Figure 1, no delamination was observed in the current A-type or prebaked B-type pucks, as illustrated in Figure 12 for B samples with 100°C/7 days annealing.

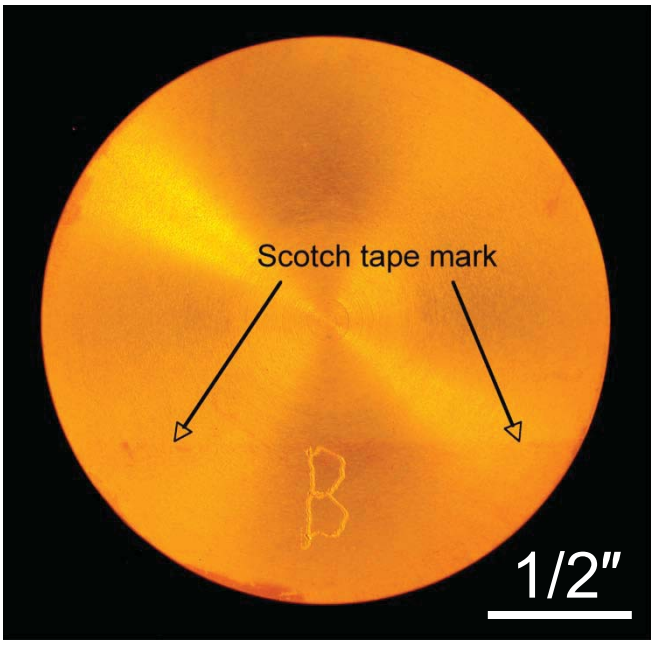


**Figure 12.** Scotch tape pull test showing that the Au coating still adhered well to the 304L substrate for the puck after 100°C/7 days annealing.

## 4.6 Auger depth profiling of the Ni strike

The Auger analyses were conducted on the B-type samples before and after Ni-plating. This B-type Ni strike (washed with D-water) without Au was plated specifically to determine the foreign species using Auger analyses. Compared with the $H_2SO_4$-cleaned 304L blank, the depth profile shows that carbon and oxygen were elevated in the Ni strike (Figure 13a–b).

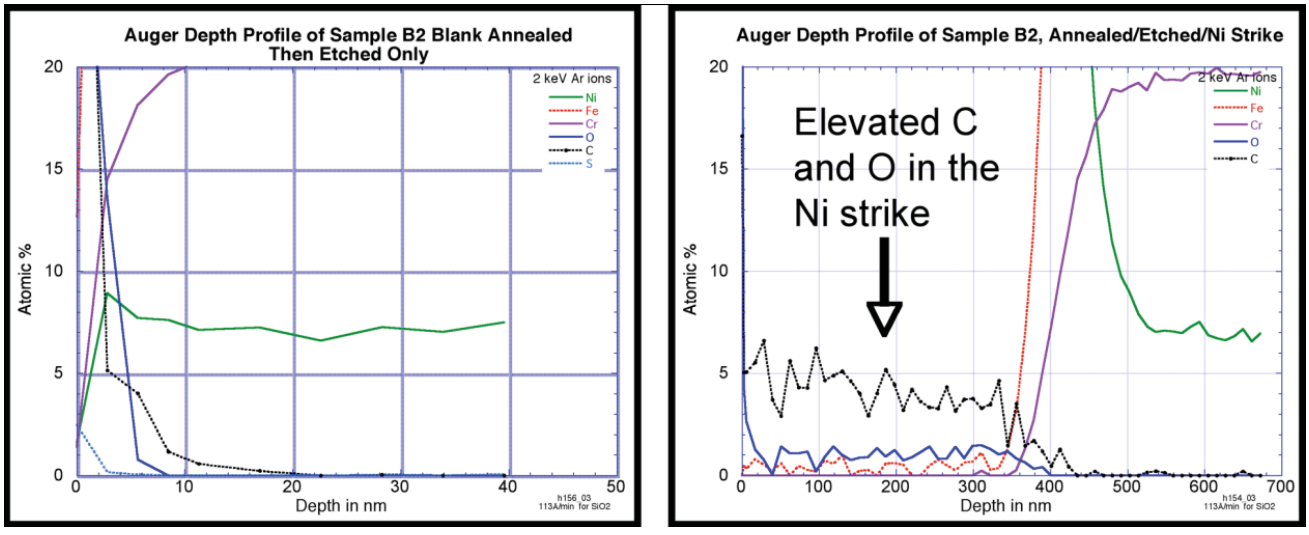


**Figure 13.** Auger depth profiles show the near-surface chemical composition. Upper left: $H_2SO_4$-cleaned B blank; Upper right: Ni strike on the $H_2SO_4$-etched B-type 304L blank.

## 4.7 Auger chemical depth profile through the Au/Ni/304L system

Auger *x*-ray depth profiling shows the similarity in the thickness of the Au coating and Ni strike layer, estimated earlier from FIB imaging, i.e., ~400–500 nm and 200–300 nm, respectively. Most significantly, the profiles consistently show carbon, oxygen, and possibly $H_2$ elevation in the Ni strike on the as-plated pucks, as well as those annealed up to 190°C/7 days (Figure 14a–f).

At 250°C for 63 days annealing, the Auger profile shows that oxygen was still elevated but carbon had diminished in the Ni strike (Figure 14g–h). At 250°C/63 days, the carbon level is slightly elevated in the 304L bulk near the Ni/304L interface. This implies that carbon in the Ni strike could have diffused back to the 304L substrate (Figure 14g–h, arrows). It is unclear how the $H_2$ evolved at this relatively higher annealing temperature. (Note that H and process liquid, e.g., $H_2O$, are undetected by Auger analysis.) However, the presence of H and $H_2O$ were indirectly confirmed in a separate study of the same Au/Ni/304L system using thermal desorption analysis/mass spectroscopy (Figure 15) (Ref. 5).

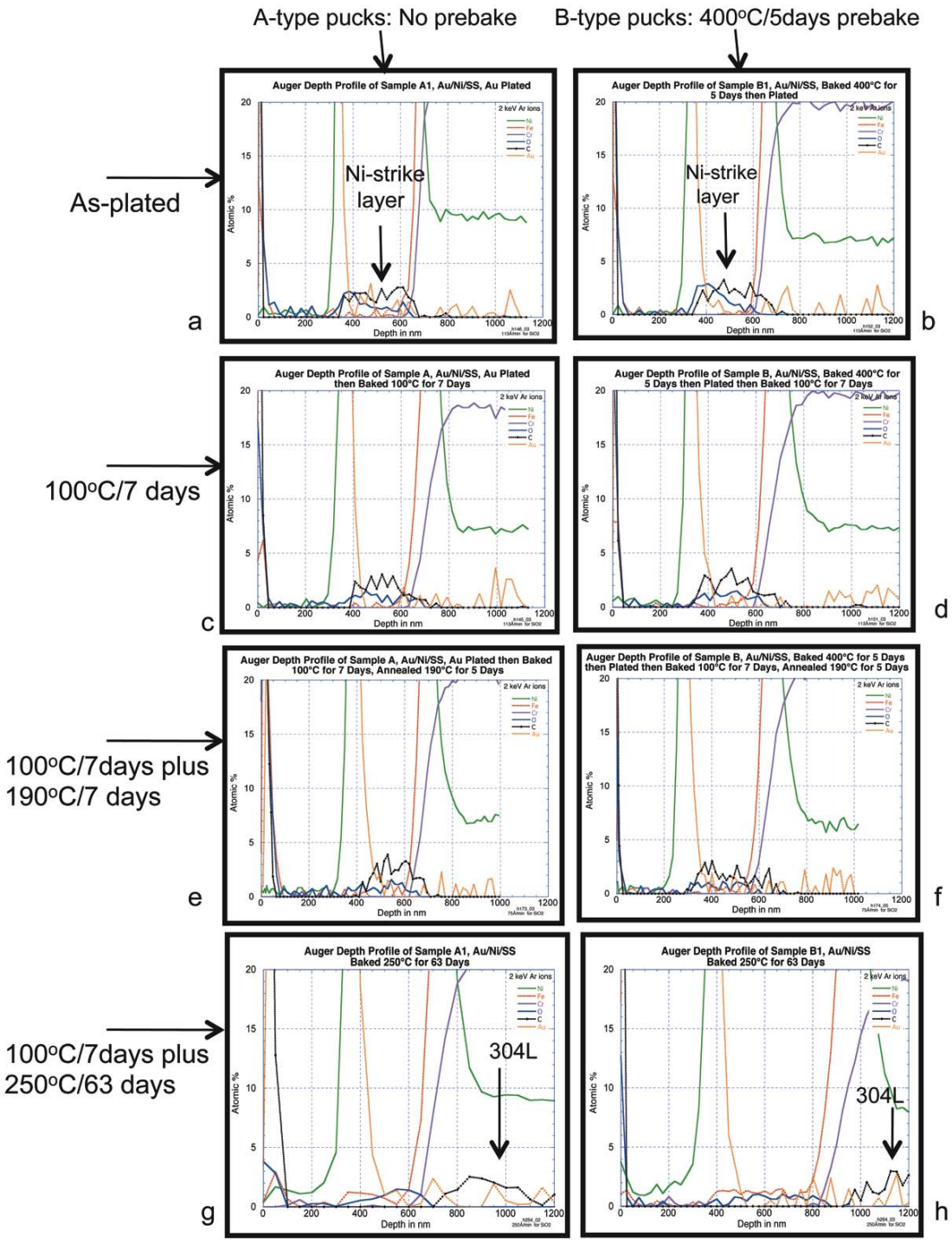


**Figure 14.** (a–f) Auger depth profiles showing elevated C and O in the Ni strike under Au coatings, including both as-plated and annealed up to 190°C/7 days. (g–h) At 250°C/63 days, the carbon content in the Ni strike is much diminished, but remains elevated in the 304L near the Ni/304L interface.

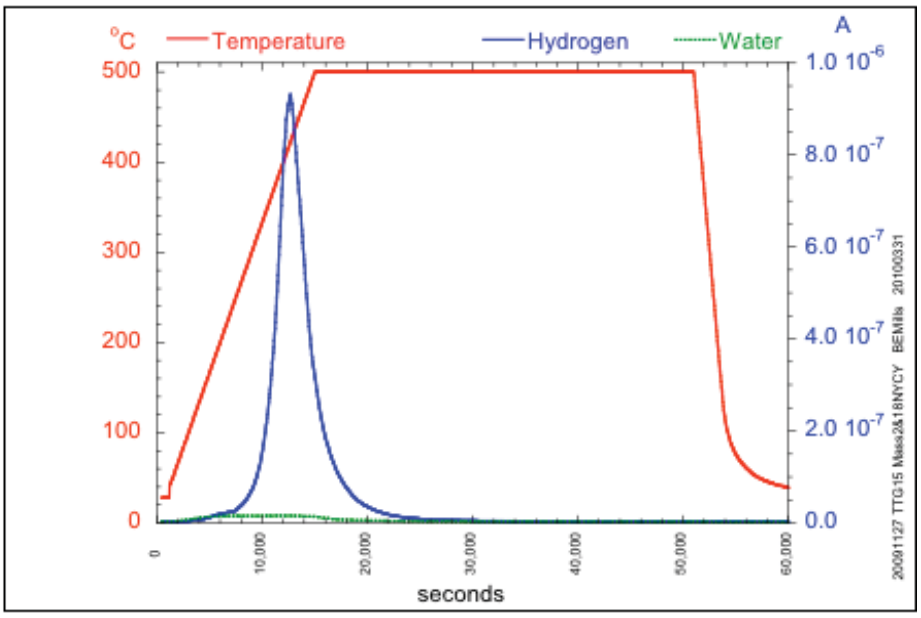


*Courtesy of B. Mills*

**Figure 15.** H and $H_2O$ detected by mass spectroscopy in the Au/Ni/304L system plated with the same plating process and condition.

## 4.8 Thermal stability of microstructure and integrity of the Au/Ni/304L system

### *4.8.1 Coating integrity and dimension by FIB imaging*

FIB images show that the typical thicknesses of the Au coating and Ni strike layer are 400–500 nm and 200–300 nm, respectively (Figure 16–17).

FIB images of the A-type samples annealed under various conditions show that the Ni and Au coatings are uniform and continuous along the Ni/Au and Ni/304L interfaces in all cases. No obvious interface discontinuity or separation exists between the Au and Ni coating seen in the FIB images at the higher magnification (Figure 16, light boxed areas) at any annealing condition. The grain structure of both Au and Ni are submicrometer in size. FIB imaging did not resolve any changes in grain structure of Au and Ni strike upon thermal annealing. Note that any nanometer-scaled pores could only be resolved by TEM, not by FIB.

Most significantly, changes in the nanopore size and distribution are seen with changes in the annealing condition. For the Au/Ni/304L system annealed at ≥190°C for ≥7 days, relatively large pores (≥50 nm) were visible, mostly within the Ni strike layer away from the interface (Figure 16, lower rows). These relatively large pores were not seen in the as-plated Ni strike (Figure 16, upper row). The pore size appeared to increase with annealing temperature from 190°C/7 days to 250°C/63 days. The pore diameter in the sample with 250°C/63 days annealing was as large as ≥100 nm, which is about one-third to one-half the thickness of the Ni strike layer (Figure 16, bottom arrows).

A similar pore evolution up to 190°C/7 days was also observed in the B-type Ni strike (Figure 17, arrows). FIB imaging of the sample with 250°C/63 days annealing was not performed initially due to resource limitations at that time. It is expected that that the pore evolution at 250°C of the B-type sample would behave similarly.

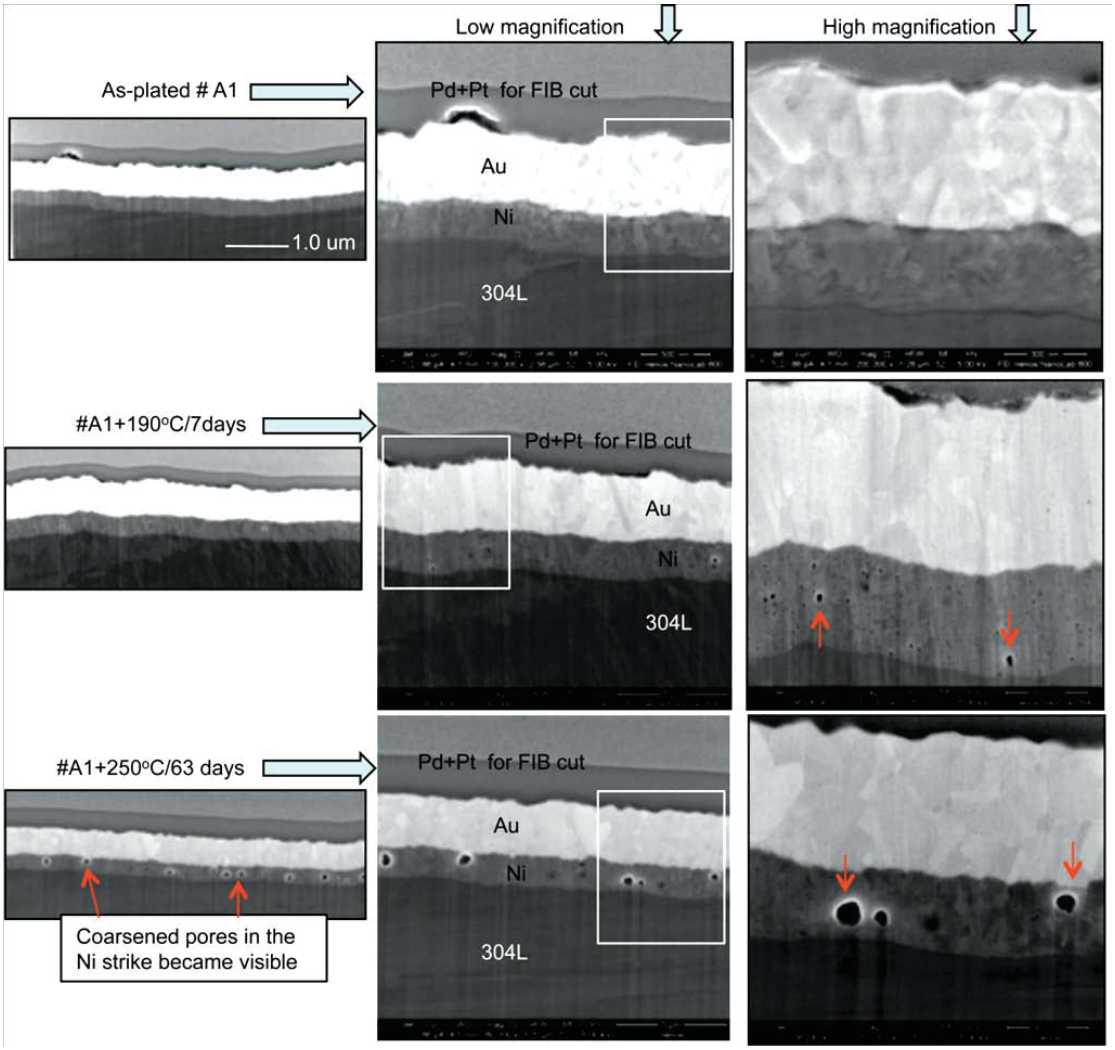


**Figure 16.** FIB images show pore coarsening in the Ni strike layer.

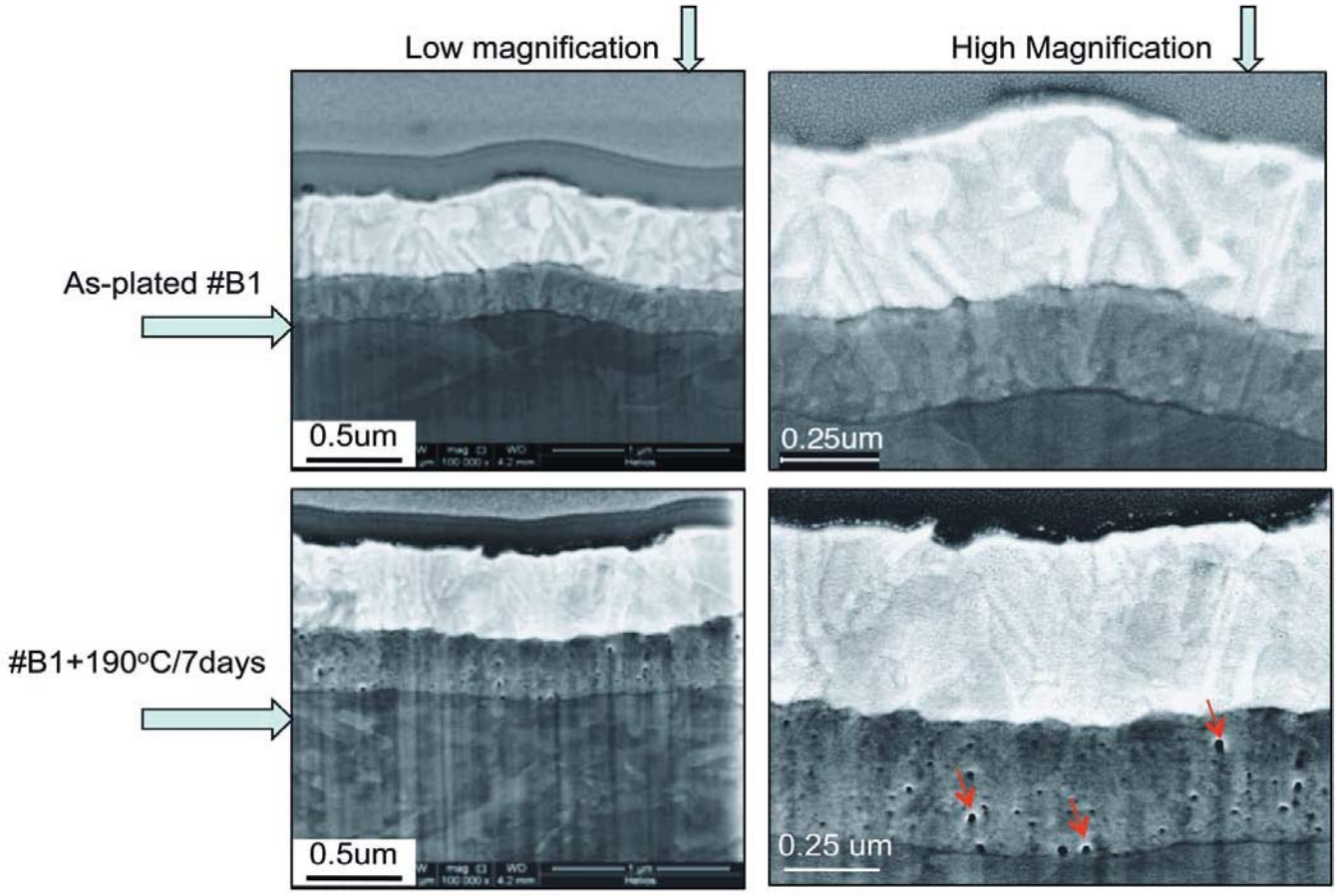


**Figure 17.** FIB images show large pores formed in the B-type sample upon thermal annealing up to 190°C/7 days. Note: The vertical curtain-like features seen on the lower left image are an artifact of uneven FIB thinning.

### *4.8.2 Au and Ni coating microstructure and integrity by TEM imaging*

TEM analysis was conducted on all eight Au-coated samples, including both the as-plated and annealed samples. The results show a comparable microstructure, e.g., grain structure and porosity and their thermal evolution, between the A-type and B-type. (The data illustrated and discussed in this section focus on the B-type samples, with 400°C/5 days prebaked.)

**As-received Au coatings and Ni strike**

TEM images show good uniform bonding at the Au/Ni and Ni/304L interfaces (Figure 18a, arrows) and the Au coating appears to be fully dense (Figure 18c). At higher magnification the images clearly show that the Ni strike was intertwined with the 304L and Au coating at both interfaces (Figure 19a–c, arrows). On the other hand, the Ni strike is quite porous, porosity estimated to be ~5–10 vol.%, based on the TEM image in Figure 19b. The pores are nanometers in size. In most cases, the pores lined up to become interconnected columnar stringers $\leq$10 nm wide and >>10 nm long (Figure 18b, arrow).

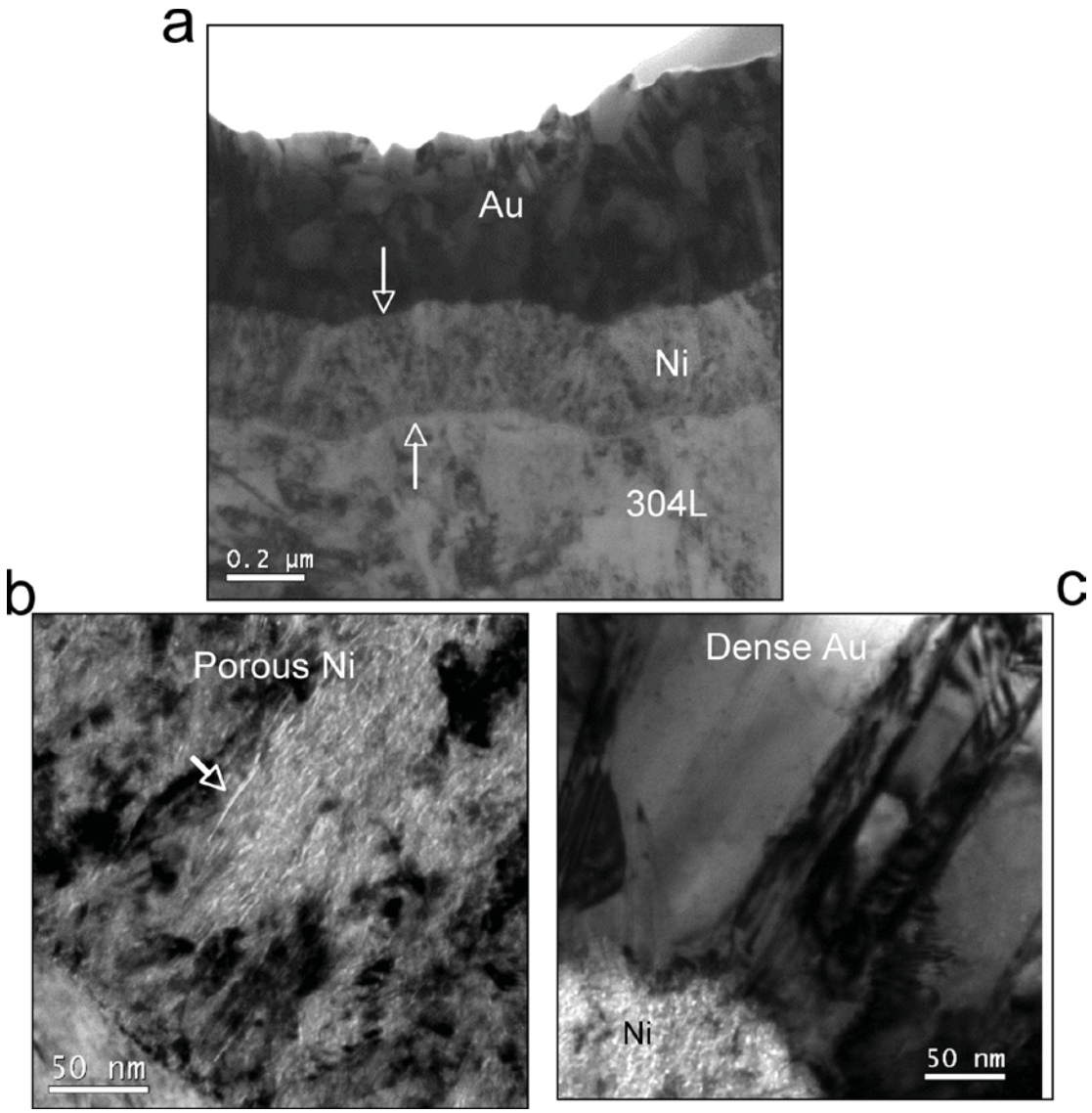


**Figure 18.** TEM images showing the typical microstructure of the as-plated Au coating.

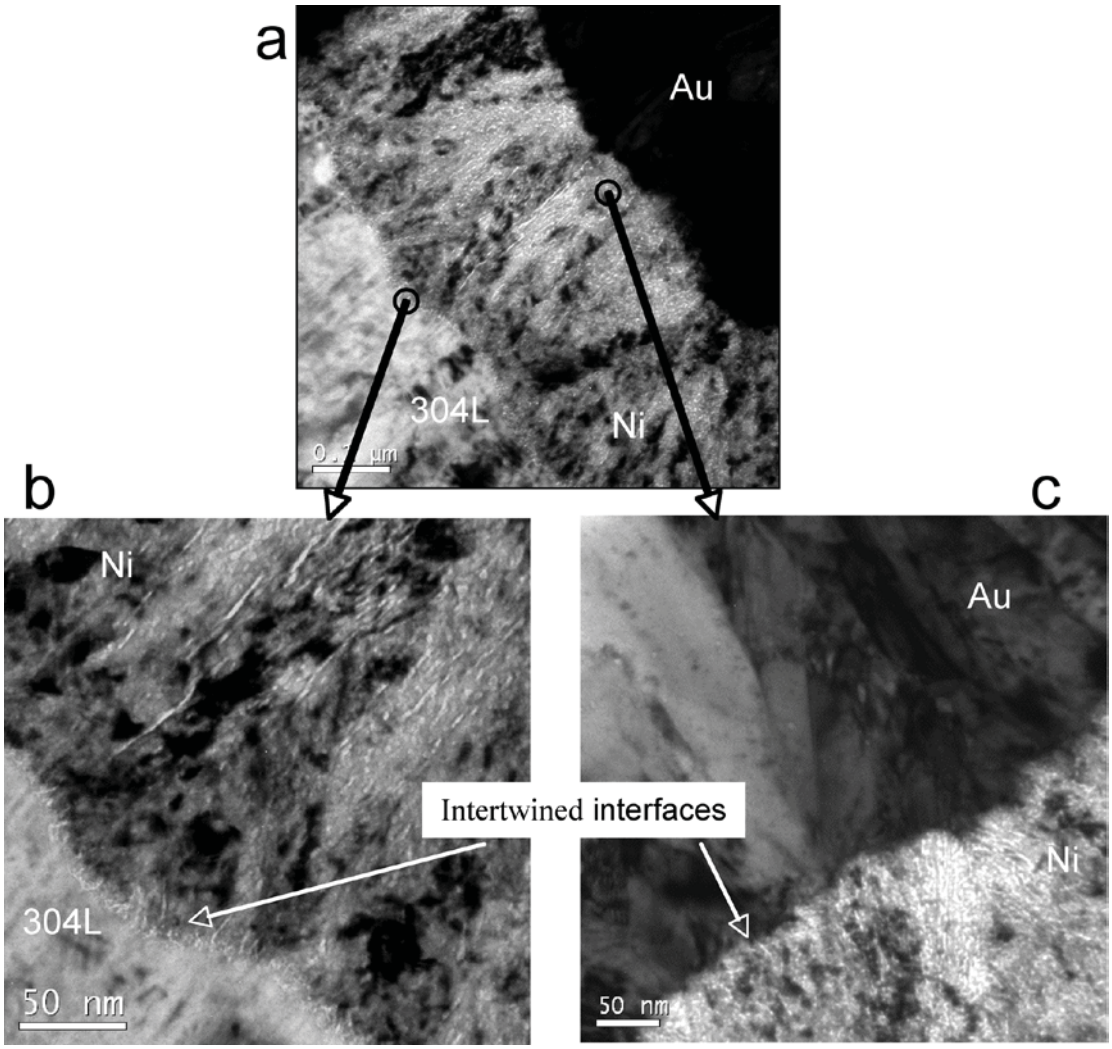


**Figure 19.** TEM images showing the Ni strike intertwined at the interfaces. (a) Overall 304/Ni/Au layered structure; (b) Ni/304L interface; (c) Ni/Au interface.

## 4.9 TEM analyses of the thermal stability of the Ni strike

TEM analyses were performed to examine the microstructure of the A- and B-type samples annealed at 100°C/7 days and 190°C/7 days. An additional experiment and analyses were also conducted to examine the microstructure evolution up to 250°C/63 days for the A-type Ni strike.

### *4.9.1 Microstructure evolution of B-type Ni strike up to 190°C/7 days*

TEM images show changes in pore dimension and morphology from those in the preexisting columnar thin stringers in the Ni strike (Figure 19a and 19d). The thin columnar pore stringers appeared to coarsen, i.e., increase in width and/or decrease in aspect ratio, as the annealing temperature increased (Figure 20a–h).

In addition, the coarsening of the pores appeared to be more pronounced along the columnar Ni grain boundaries (Figure 20c, arrow). At 190°C/7 days annealing, the pores along the grain boundaries seemed to increase to ≥30 nm (Figure 20c and 20f, arrows) which is five to ten times larger than those pore stringers seen in the as-received Ni strike.

It is unclear whether or not the volume fraction of pores changed before and after annealing. A comparison of porosity before and after annealing was not made due to the difficulty in resolving the pores in the highly complex TEM images.

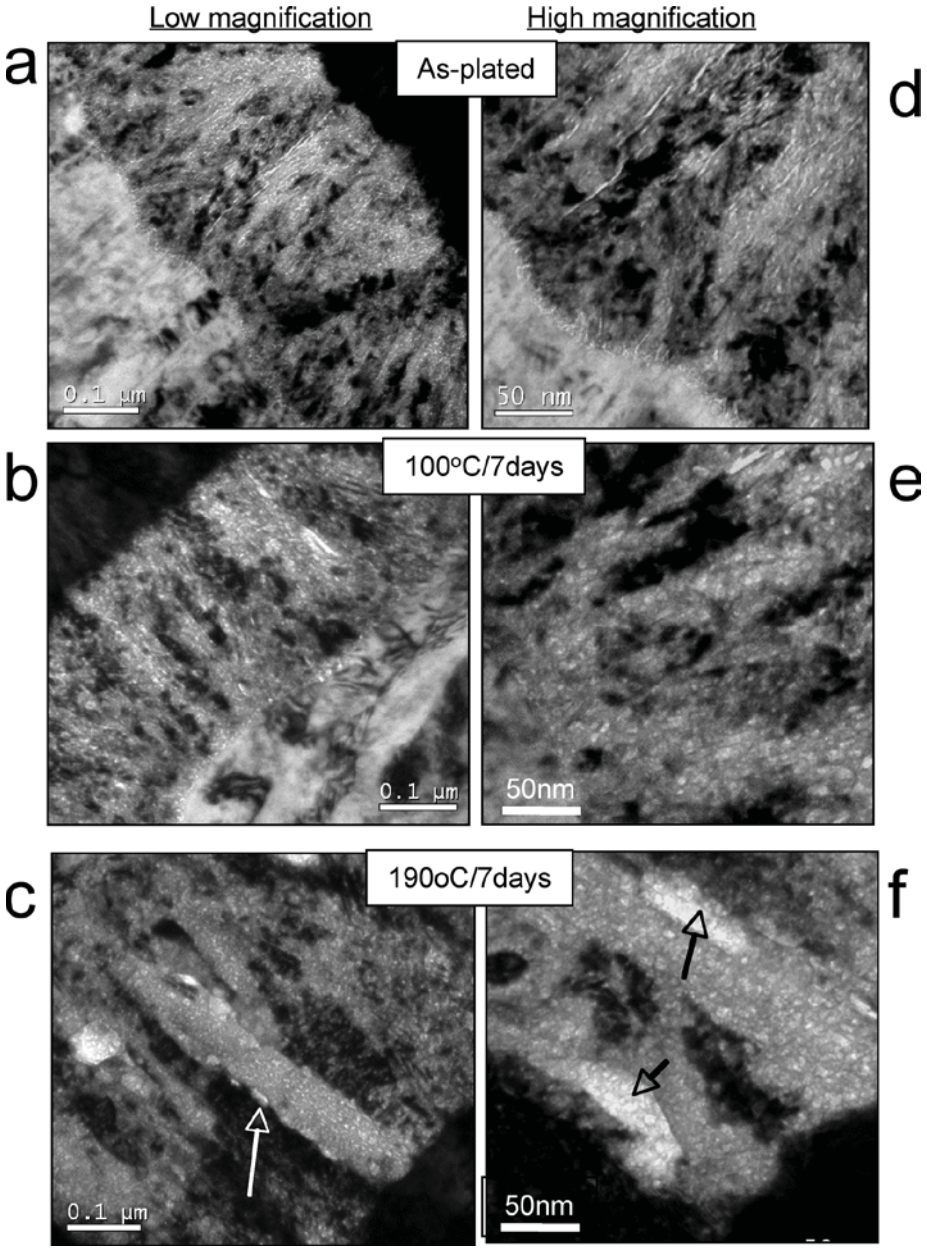


**Figure 20.** TEM images showing microstructure and nanopore evolution of the B-type sample with annealing temperature; (a–c) at low magnification; (d–f) at high magnification.

### *4.9.2 Microstructure evolution of A-type Ni up to 250°C/63 days*

TEM analyses show similar nanopore coarsening in the B-type Ni strike upon annealing up to 190°C/7 days (Figure 21a–f). For instance, see 190°C/7 days, where the large pores (≥50 nm) were formed mostly along the columnar grain boundaries (Figure 21e).

Most significantly, at 250°C/63 days, the pore coalescence and coarsening became substantial. A montage of low-magnification TEM images shows that the enlarged pores extend throughout the entire TEM sampling area (Figure 22). In addition, the diameter of the greatly coarsened pores varied from 100 nm to 300 nm (Figure 22, arrows). The large pores in many locations occupied almost one-third to one-half of the full Ni thickness. The greatly enlarged pores in general are equiaxed or spherical, as illustrated in the TEM images in Figure 21g–h. This TEM finding of the large pores is consistent with those seen and described in the FIB images earlier in Figure 16.

Besides the large pores, a noticeable number of fine pores, <<50 μm, were present in all of the thermally annealed Ni, including 250°C/63 days. A similar observation was made in the TEM imaging of B-type Ni, discussed above.

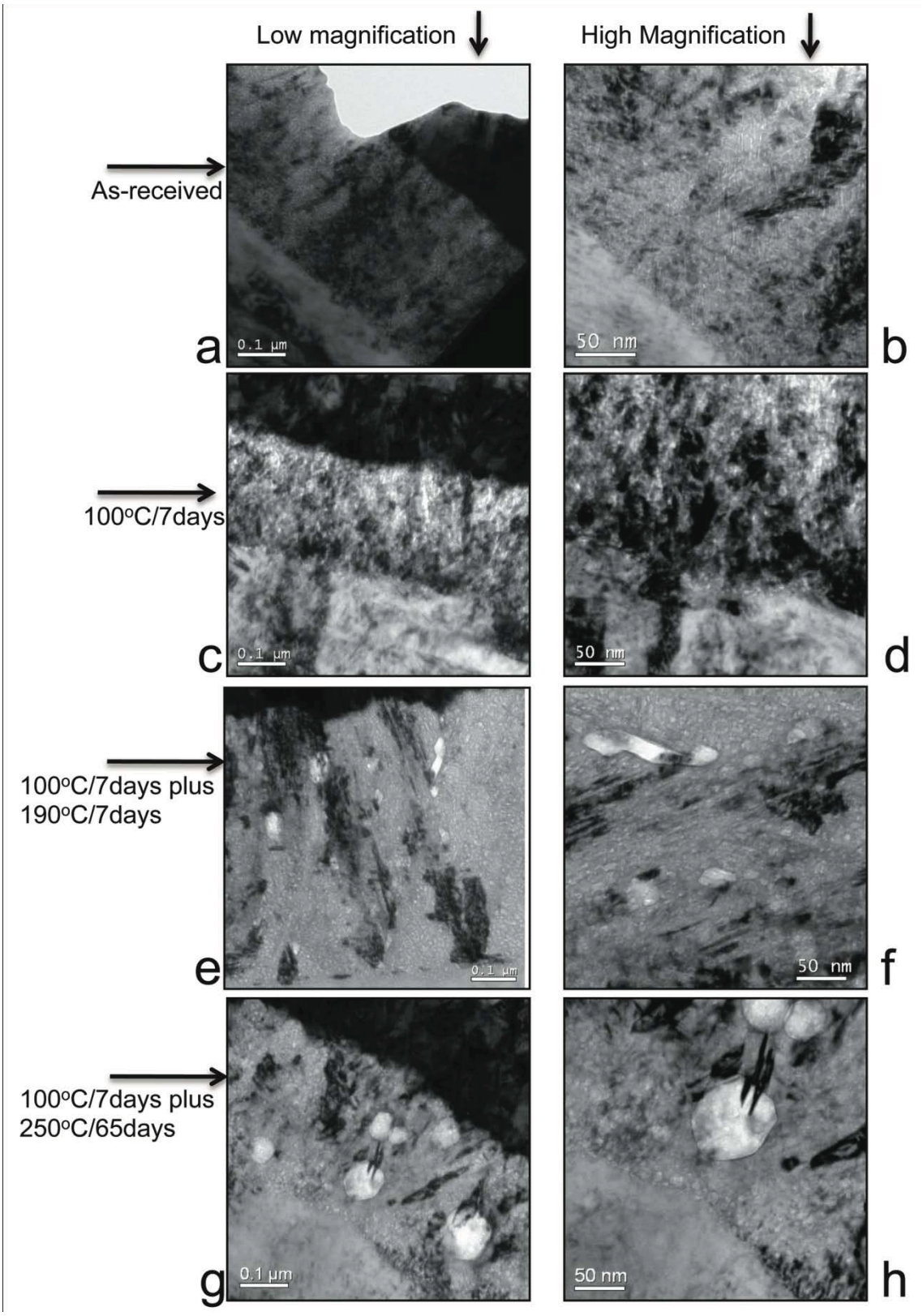


**Figure 21.** TEM images showing pore coarsening in an A-type Ni strike up to 250°C/63 days.

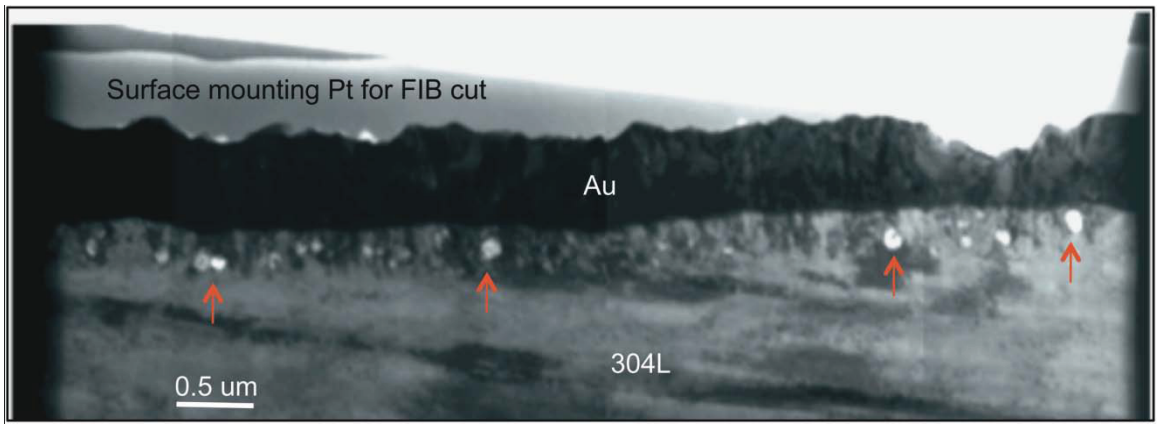


**Figure 22.** Montage of TEM images of the A-type Ni showing moderate population of large pores (see arrows) that are one-third to one-half of the Ni strike thickness.

### *4.9.3 Microstructure evolution of Au coating by TEM imaging*

TEM analyses were conducted on the A- and B-type Au coatings. There was little difference with respect to the initial microstructure and its thermal evolution between the A- and B-types.

**As-plated grain structure and porosity of the B-type**

TEM results show the as-plated Au coating in general contains nanoscale grains that are thermally stable upon annealing. TEM images show that the as-plated B-type Au coating possesses a submicron-sized grain structure, 50–300 nm (Figure 23a). The detailed TEM analyses show the presence of extremely fine nanopores (≤10 nm) distributed non-uniformly within some of the seemingly 100% dense as-plated Au matrix. In some cases, the nanopores were barely visible within the grain and some are visible along the grain boundaries (Figure 23a, arrows).

**Thermal stability of microstructure and nanopores**

The TEM/FIB study shows a relatively stable grain structure upon thermal annealing. There is no evidence of recrystallization. However, the TEM images seem to suggest a slight increase in size and population of the nanopores as the thermal annealing temperature increases (Figure 23a–d). The changes in size, morphology and population of the nanopores in the Au coating were not nearly as significant as those seen in the Ni strike. In general, the pore size in all of the annealed Au coatings, including the 250°C/63 days, varied from 10–25 nm, which is difficult to resolve by FIB imaging. Note that the nanopores mostly resided along grain boundaries (Figure 23b–c, arrows).

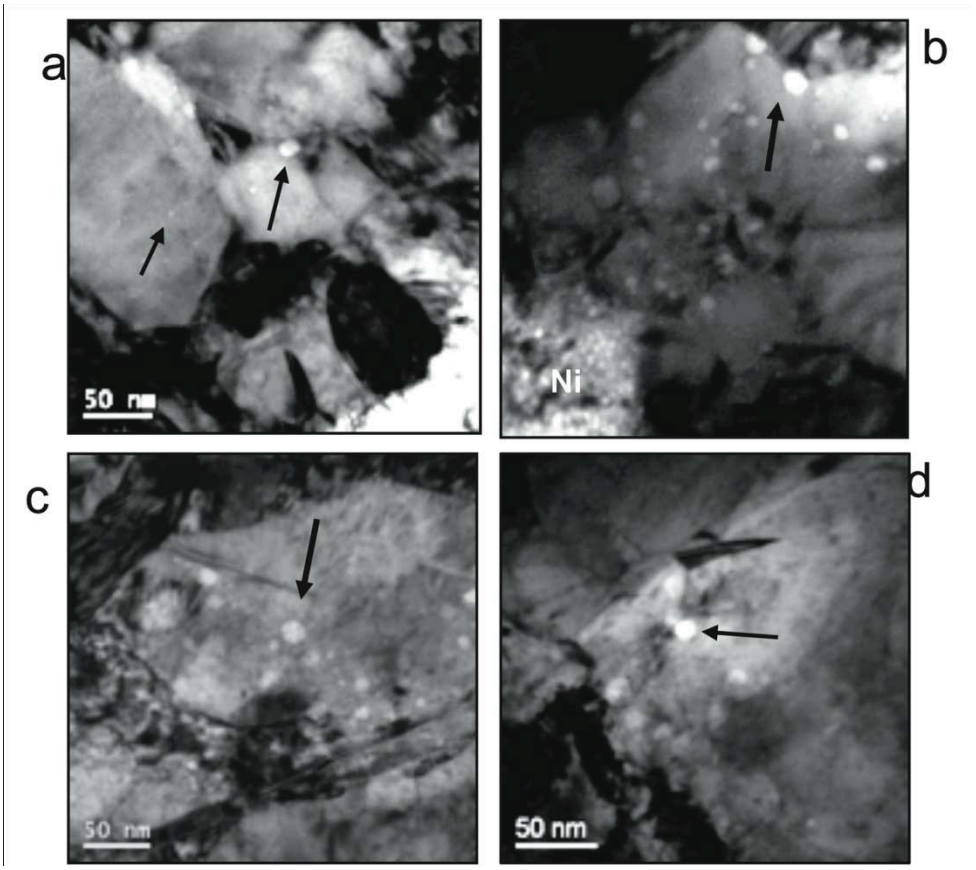


**Figure 23.** TEM images of the Au coating; (a) as-plated; (b) 100°C/7 days; (c) 190°C/7 days; (d) 250°C/63 days (A-type).

### *4.9.4 Chemical evolution upon thermal annealing*

The chemical composition changes in A-type Ni and Au across the Au and Ni thicknesses, respectively, were calculated from the *x*-ray intensity measured using TEM/EDS analyses.

**Ni-diffusion into Au coating**

For the as-plated A-type samples, the average Ni concentration in the Au coating is ~0.1 wt%, while the Ni peak was barely visible in the EDS spectrum (Figure 24 and Table 4). Such low Ni concentration may not be statistically significant because the extremely low *x*-ray intensity yield approaches the detection limit of EDS analysis. The presence of C, Cu and Fe are artifacts due to a combination of the electron beam exposure to carbon buildup, the supporting Cu grid, and *x*-ray fluorescence of the TEM pole piece.

Upon annealing, EDS showed the average Ni concentration in the Au coating increases from 0.12 wt% in the as-plated samples to 0.62 wt % at 190°C/7 days (Table 4, bottom row). The Ni concentration across the Au layer at various annealing conditions showed a clear trend of decreasing Ni from the Ni/Au interface to the Au surface (Figure 25).

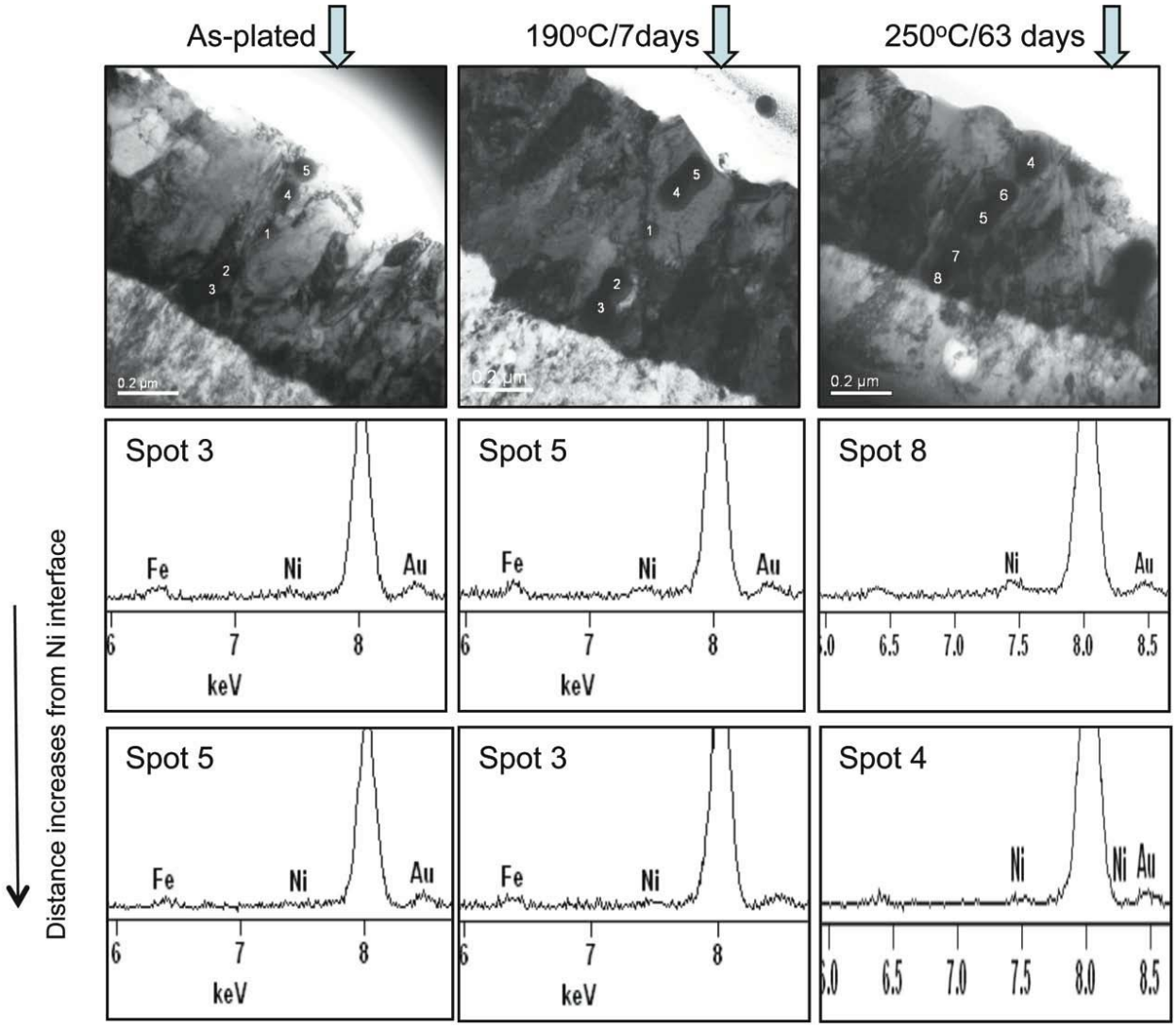


**Figure 24.** EDS shows the Ni diffusion.

**Table 4.** Ni concentration changes with distance and temperature by TEM/EDS in as-plated A-type samples.

| ***As-plated*** | | ***190°C/7days*** | | ***250°C/63 days*** | |
|---|---|---|---|---|---|
| Distance (nm) | Ni(wt%) | Distance (nm) | Ni(wt%) | Distance(nm) | Ni(wt%) |
| 97 | 0.3 | 96 | 0.42 | 50 | 0.97 |
| 189 | 0.05 | 185 | 0.11 | 127 | 0.71 |
| 364 | 0.11 | 384 | 0.42 | 264 | 0.53 |
| 510 | 0.16 | 538 | 0.27 | 364 | 0.46 |
| 610 | 0 | 623 | 0.28 | 485 | 0.41 |
| Average Ni wt% | 0.12 | | 0.30 | | 0.62 |

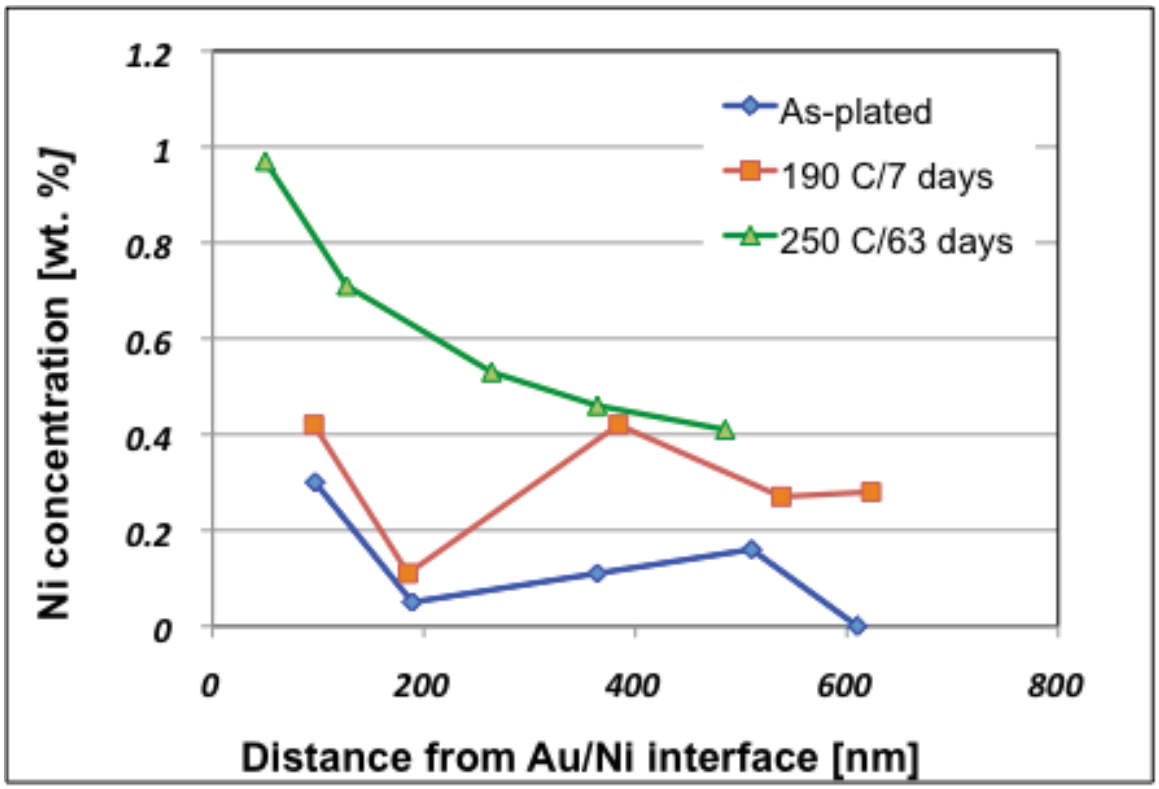


**Figure 25.** Diffusion profile of Ni at various annealing temperatures. Ni diffusion depth profiling shows increased Ni concentration with annealing temperature.

**Au diffusion into Ni coating by qualitative TEM/EDS analysis**

TEM images and EDS spectra pairs show a possible shallow Au diffusion into Ni, <100 nm deep from the Au/Ni interface (Figure 26). This Au diffusion into Ni using EDS is not conclusive due to a possible artifact of *x*-ray fluorescence from the nearby thin Au coating.

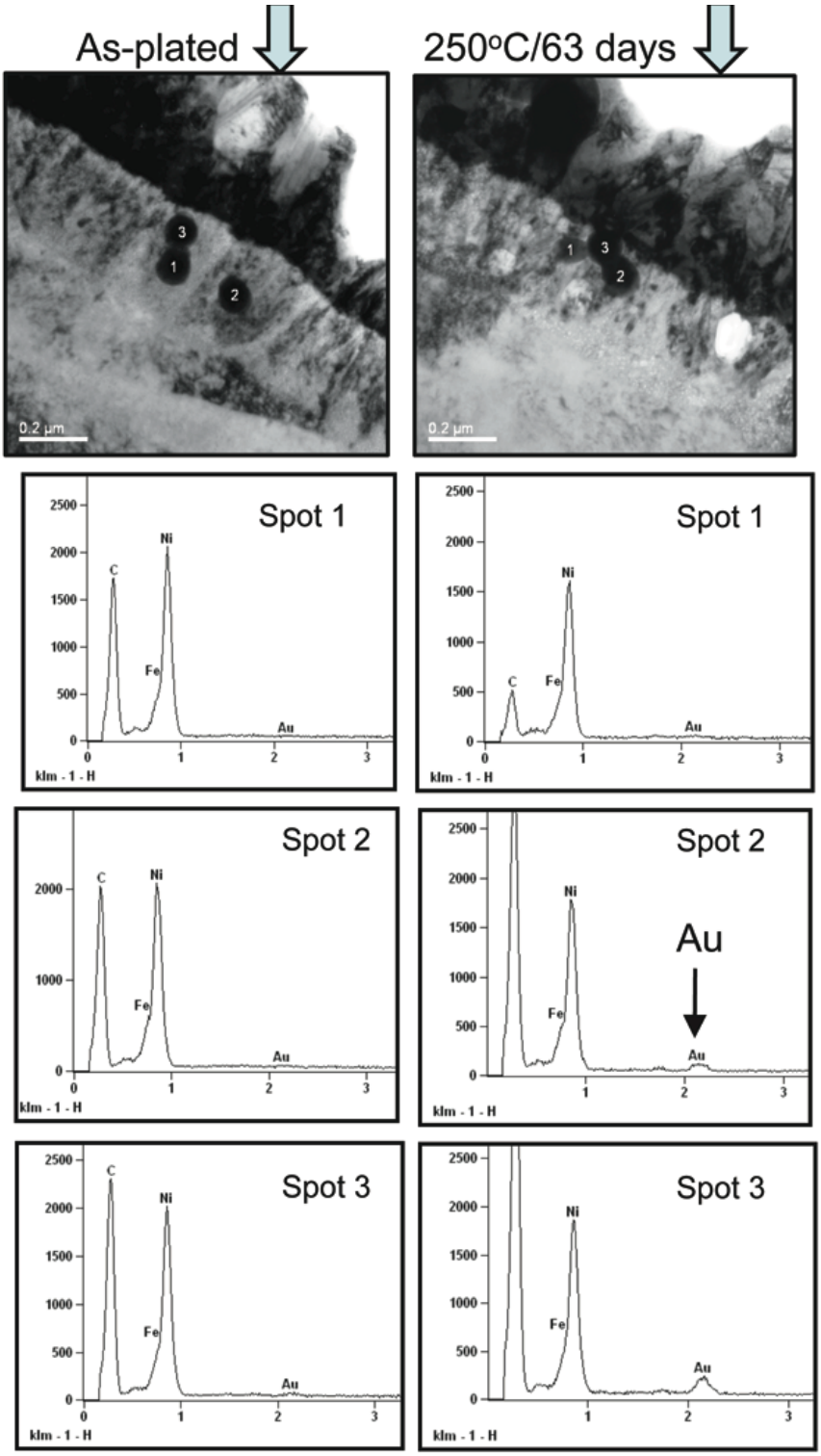


**Figure 26.** (Upper) TEM images showing the location of EDS analyses; (lower) EDS spectra showing the presence of Au in the Ni strike annealed at 250°C/63 days and the absence of Au in the as-plated Ni strike.

# 5 Summary and Discussion

Electron optical imaging shows the as-plated Au coatings are close to 100% dense with a minor amount of nanopores (<<10 nm), and the Au/Ni and Ni/304L interfaces exhibit good bonding. Upon thermal annealing up to 250°C/63 days, the grain structure of the Au and Ni coatings remains unchanged and the Au/Ni and Ni/304L interfaces remain well-bonded. The nanopores in the Au coating appear to have little effect on the Au/Ni/304L system integrity and/or interface bonding upon thermal heating. The good adhesion is most likely attributable to good mechanical locking between the porous Ni strike and the rough mechanical surface finish of the 304L substrate (Figure 27).

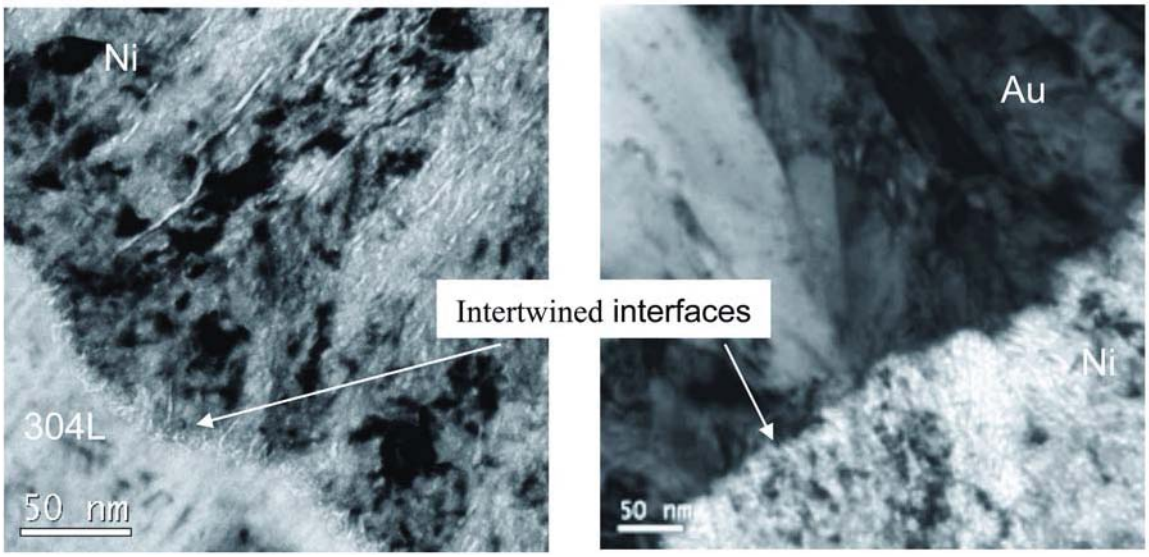


**Figure 27.** High volume fraction of nanopore stringers and intertwined interfaces from good mechanical locking.

The surface finishing from the mechanical milling or $H_2SO_4$ cleaning seems to affect the crystal morphology and surface roughness of the Ni strike. However, the consistently good Ni/Au interface bonding among all A- and B-type samples suggests a minimal effect of Ni strike surface finishing on the mechanical locking, which is the source of the good adhesion.

The Wood's Ni strike is porous and contains 5–10 vol.% in the form of interconnected fine stringers, <<10 nm in width (Figure 27, left). The porous Ni strike is susceptible to trapping foreign substances such as processing liquid that contains carbon, oxygen, water, and hydrogen bubbles from electroplating (Figure 28a–b). Upon thermal annealing, the entrapped foreign substance(s) persist in the Ni strike (Figure 28c–d) and the nanosized columnar pores coarsen (Figure 29a–f). The nanopore coarsening presumably is attributable to a combination of Oswald ripening of the gaseous phase(s), including $H_2$, and vacancy diffusion during thermal annealing. In the extreme case, 250°C/63 days, the pores were enlarged up to ≥300 nm, or approximately one-third to one-half of the Ni thickness.

How this pore coarsening and foreign substances entrapment affect outgassing, long-term reliability and integrity of the Au/Ni/304 system is yet to be determined. In order to mitigate the nanopore aggregation and/or coarsening, thermal annealing at >200°C< 400°C after Ni strike, prior to Au plating, is recommended In order to eliminate the outgassing species at elevated temperature.

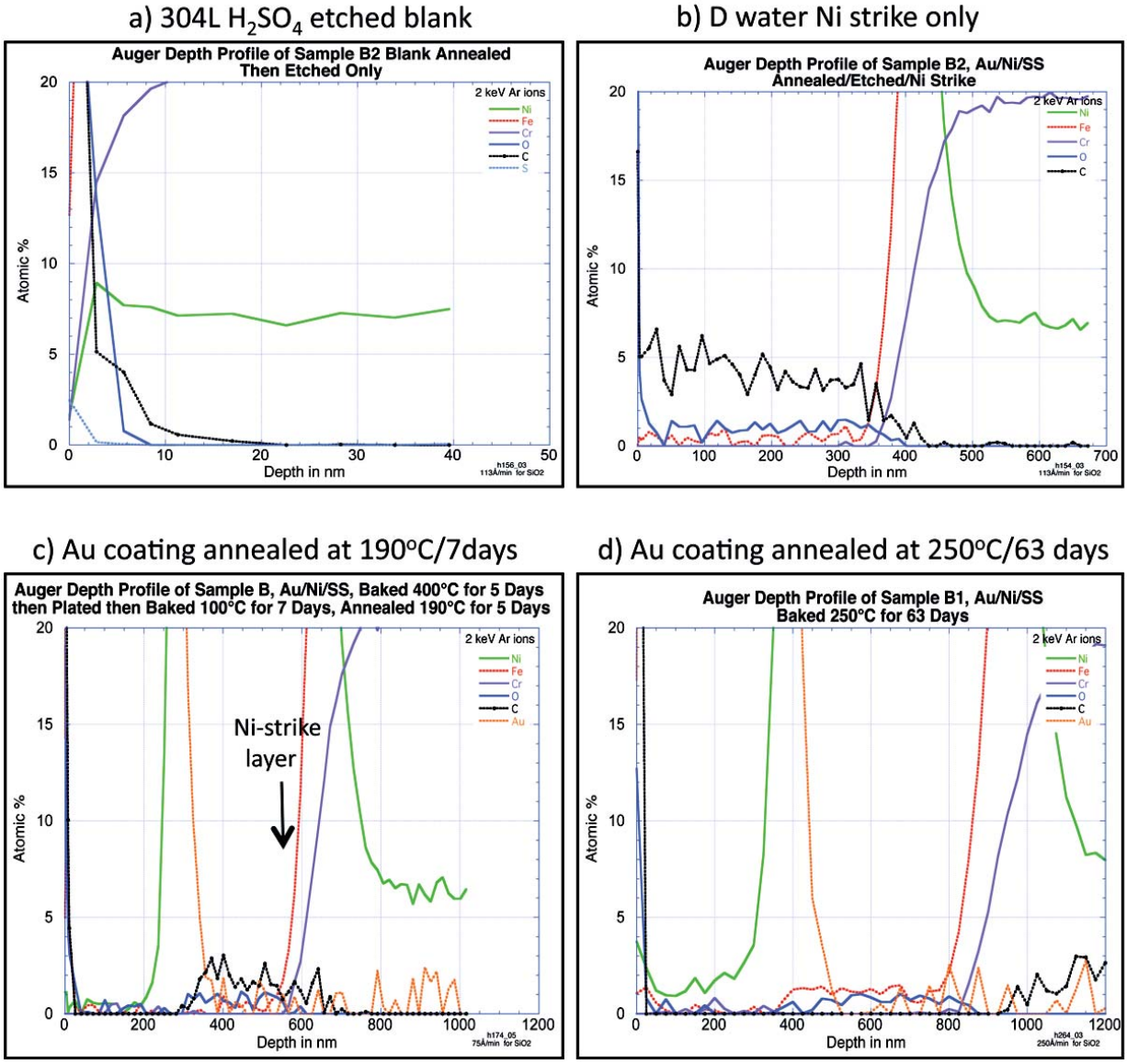


**Figure 28.** (a–c) Auger depth profiles showing the presence of C and O in the porous Ni strike at ≤190°C/7 days; (d) After 250°C/63 days annealing, the remaining oxygen in the Ni strike and C appeared to diffuse into the 304L.

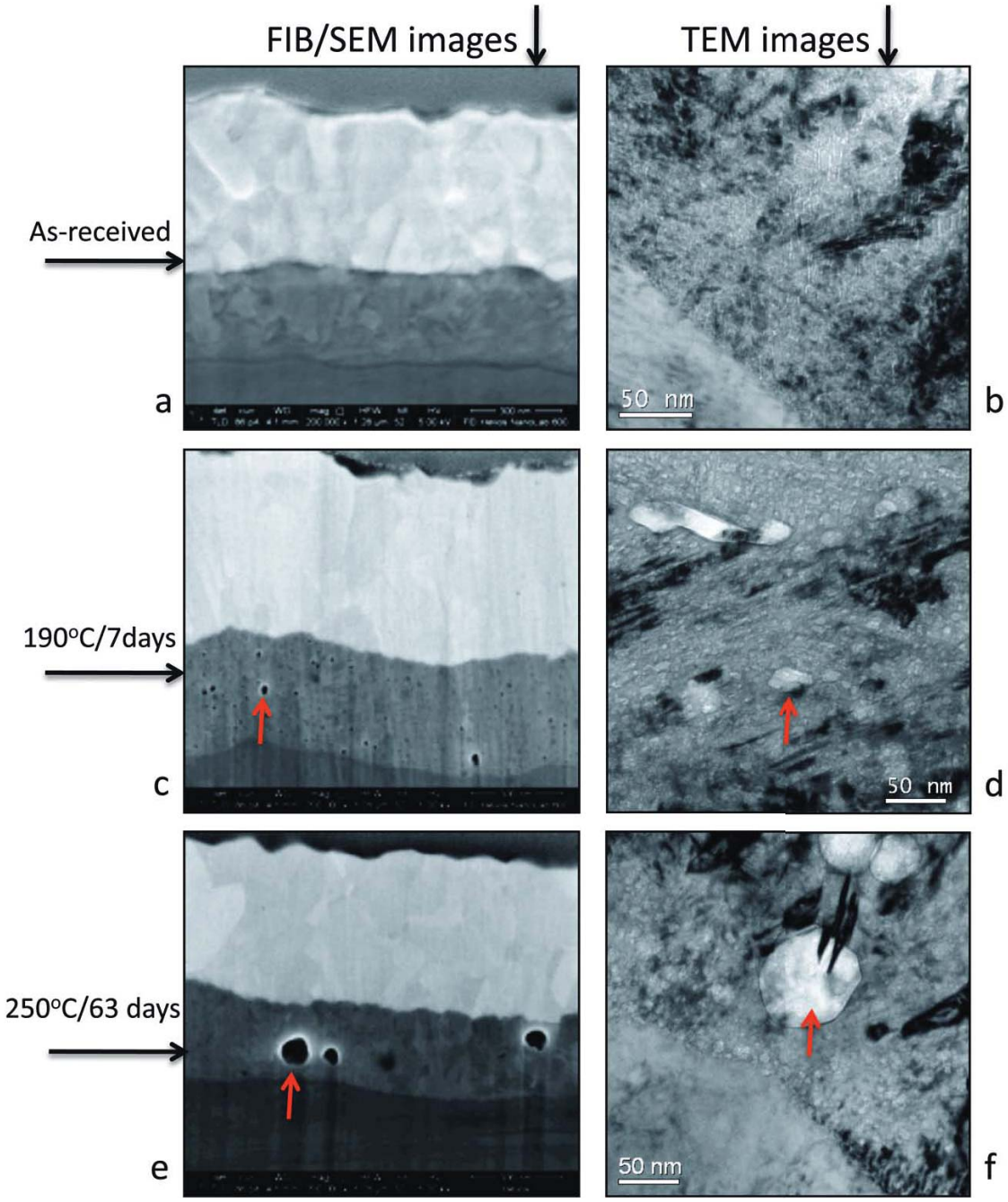


**Figure 29.** FIB/SEM and TEM imaging of pore coarsening in the porous Ni strike.

Ni diffusion into Au is evident and the concentration of Ni increases with the annealing temperature. How the presence of Ni in the Au coating affects the Au emissivity is yet to be understood.

The step of 400°C prebake for H-removal from the 304L blank is susceptible to Cr-oxide formation. The oxide formation is evident from surface discoloration seen in the two separate studies (Figure 30). The Cr-oxide was observed when the 304L blanks were prebaked at

$\geq 1 \times 10^{-4}$ Torr with a mechanical pump, but it was not seen when baked at $1 \times 10^{-8}$ Torr by turbo pump.

Presence of a thin surface oxide could have an adverse effect on the H-removal if oxidation occurs early in the prebake before to $H_2$ has a chance to escape. This may be the reason why we observed similar pore evolution in the Au coatings between the A- and B-types.

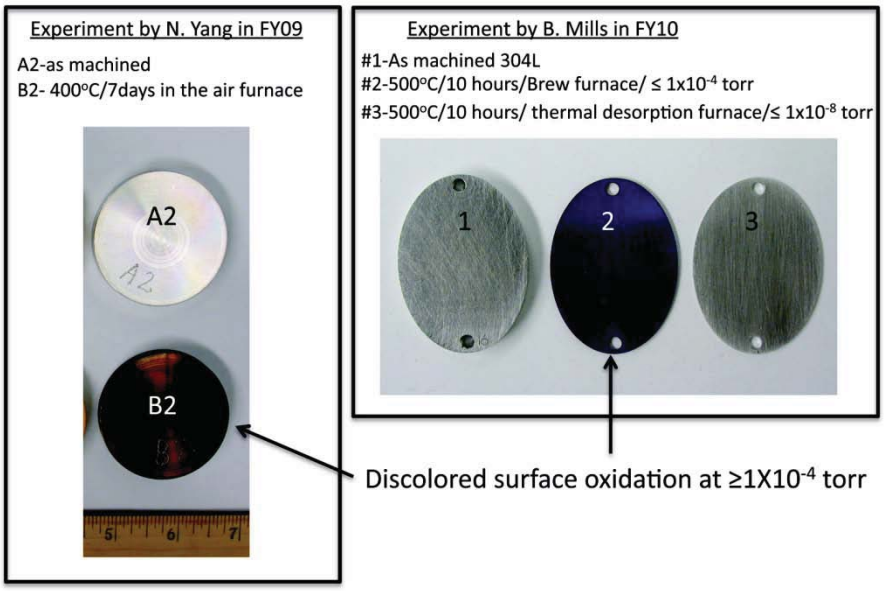


**Figure 30.** Discoloration due to Cr-oxide seen on the surface of 304L blanks prebaked at $1 \times 10^{-4}$ Torr.

# 6 Conclusions

The adhesion of the current as-received Au/Ni/304L system is adequate and is attributed to good mechanical locking between the rough 304L finish and porous electroplated Wood's Ni strike.

The Ni strike contains a high volume fraction, 5–10 vol.%, of nanopore stringers, which renders it susceptible to trapping foreign substances such as outgassing processing liquid and $H_2$ gas. These nanopores stringers and the entrapped outgassing substances are thermally unstable. Upon thermal heating, the pores coalesced, leading to pore coarsening of up to one-half of the Ni strike thickness at the extreme case. The extent of pore coarsening in the Ni strike and its effect on the long-term Au/Ni/304L system integrity and adhesion is yet to be understood.

Moderate Ni diffusion into Au was evident in the sample annealed at ≥190°C/7 days. The effect of this Ni diffusion on the thermal emissivity of the Au is a subject for future study.

The 400°C prebake at $\geq 1 \times 10^{-4}$ Torr with mechanical pump promotes surface Cr-oxide formation, which reduces the effectiveness of the H-removal. In order to prevent surface oxidation, a surface turbo pump at $\leq 1 \times 10^{-8}$ Torr is required.

This page intentionally left blank.

# References


1. "Plating technology for electronic packaging." Hideo Honma, *Electrochimica Acta*, 47, 2001.
2. "Effect of brightness on hydrogen evolution during Zinc electroplating from zincate electrolytes." M. Monev, etc. *Journal of Applied Electrochemistry*, 28, 1998.
3. "Study of the kinetics of hydrogen evolution on Nickel-Zinc alloy electrodes." Linlin Chen, etc., *J. Electrochem. Soc*. Vol. 138, Nov. 1991.
4. "Grain boundary diffusion coefficients in the Gold-Nickel thin film." Ahmed M. Abdul-Leffit, *Surface Interface Analysis*, 35, 2003.
5. "Thermal desorption analysis for the electroplated Au/Ni/304L system." Private communication with Bernice Mill, May, 2010.

This page intentionally left blank.

# Distribution

| | | | |
|---|---|---|---|
| 1 | 8650 | Bill Even | 9161 |
| 1 | 8210 | D. Kwon | 9154 |
| 1 | 8220 | M. Hardwick | 9153 |
| 1 | 8656 | S. Allendorf | 9161 |
| 1 | 8224 | P. Spence | 9035 |
| 1 | 8223 | A. Morales | 9403 |
| 1 | 18152 | C. Apblett | 1349 |
| 1 | 2547 | S. Whalen | 0614 |
| 1 | 2547 | D. Wesolostki | 0614 |
| 1 | 2547 | M. Contreras | 0614 |
| 1 | 8365 | T. Johnson | 9409 |
| 1 | 8223 | J. Hachman | 9403 |
| 1 | 8651 | J. Chames | 9402 |
| 1 | 8651 | W. Clift | 9402 |
| 1 | 8651 | N. Yang | 9402 |
| 1 | | B. Milles | |
| 1 | 8223 | T. Shepodd | 9403 |
| 1 | 8221 | J. Jorenby | 9154 |
| 1 | 8224 | S. Rice | 9035 |
| 1 | 8222 | S. Goods | 9404 |
| 1 | 8656 | P. Sharma | 1413 |
| 1 | 8656 | D. Medlin | 9161 |
| | | | |
| 2 | 9018 | Central Technical Files | 8944 |
| 1 | 0899 | Technical Library | 9536 |